NASA TN D-5

TECHNICAL NOTE

D-5

INVESTIGATION OF METHODS FOR COMPUTING FLUTTER CHARACTERISTICS OF SUPERSONIC DELTA WINGS AND COMPARISON WITH EXPERIMENTAL DATA

By C. H. Wilts

California Institute of Technology

NATIONAL AERONAUTICS AND SPACE ADMINISTRATION

WASHINGTON

August 1959

NATIONAL AERONAUTICS AND SPACE ADMINISTRATION

TECHNICAL NOTE D-5

INVESTIGATION OF METHODS FOR COMPUTING FLUTTER CHARACTERISTICS OF SUPERSONIC DELTA WINGS AND COMPARISON WITH EXPERIMENTAL DATA

By C. H. Wilts

SUMMARY

A study was made of the flutter characteristics of two delta wings using an electric-analog computer. Comparison is made of the structural characteristics as obtained on the analog with experimental values. Using strip theory and the box method to represent the aerodynamics, the analog flutter characteristics were also compared with experimental values. A partial check of the analog procedures is furnished by a flutter analysis on a digital computer.

INTRODUCTION

The aeroelastic performance of aircraft and missiles is a subject of great practical importance. The response of an aircraft to turbulence, gusts, and maneuvers, and the basic stability problems of divergence and flutter are all aspects of this general problem. Since by definition one is concerned with interactions between the elastic properties of a structure and aerodynamic forces, it is clear that useful design computations require a reasonably accurate knowledge of both the structure and the aerodynamic forces. There are at present several powerful methods of determining and representing the structural properties of typical aircraft. However, there does not seem to be at the present time any adequate theory for computing in a practical way the actual aerodynamic pressures on a plan form of arbitrary shape undergoing arbitrary but physically meaningful deformation.

It appears that a unified theory or scheme of computation which has been verified by experimental correlation is still remote. Nevertheless there is now sufficient experimental flutter data so that it is possible to seek computation schemes and simplified aerodynamic-force representations which will give satisfactory correlation with experiment for certain plan forms. Assuming that the experimental flutter data has been obtained with reasonable accuracy, the principal additional requirement for its use

in such correlation research is that the structure of the airfoil be defined accurately. A particularly good example of research that satisfies this requirement is found in some of the plan forms investigated in reference 1. The delta wings discussed there were made of uniform thin sheets of magnesium and therefore the structure is completely known within the adequacy of plate theory except for the rigidity of the cantilever restraint. This report is devoted to a structural and flutter analysis of the delta-wing airfoils of reference 1 at supersonic speeds. In this analysis several aerodynamic representations were used to determine which gave better correlation with the experimental flutter data of reference 1.

This investigation was conducted at the California Institute of Technology under the sponsorship and with the financial assistance of the National Advisory Committee for Aeronautics.

SYMBOLS

A	aspect ratio
C_{L_q}	lift coefficient for pitch
C_{L_α}	lift coefficient for angle of attack
C_{M_q}	moment coefficient for pitch
C_{M_α}	moment coefficient for angle of attack
$\left\{C_{L_\alpha}(\tau)*\alpha(\tau)\right\} \equiv \int_{-\infty}^{\tau} C_{L_\alpha}(\tau - X)\frac{d}{dX}\alpha(X)dX$	
c	local chord of wing in airstream direction
E	modulus of elasticity, lb/sq in.
F	aerodynamic lift force, lb
f	frequency, cps
g_1, g_2	structural damping of normal modes

h	vertical deflection of wing, in.
$i = \sqrt{-1}$	
k_{ij}	function representing pressure at station (j) due to wing deflection at station (i)
M	moment
Ma	Mach number
P_0, P_1, P_2	pressure coefficients defined in appendix B
p	pressure, lb/sq in.
q	dimensionless pitching velocity, $\frac{c}{v}\dot{\theta}$
S	area, sq in.
t	wing thickness, in.
v	free stream air velocity
w	downwash, $w = \theta v + \dot{h}$
x, ξ	chordwise coordinate on wing
x_o	dimensionless per unit chord location of aerodynamic center behind leading edge
x_1	dimensionless per unit chord location of rotation center behind leading edge
y, ζ	spanwise coordinate on wing
α	angle of attack, radians $\alpha = \theta + \frac{\dot{h}}{v}$
β	supersonic coefficient, $\beta = \sqrt{Ma^2 - 1}$
ΔS	area of finite-difference cell, sq in.
Δx	chordwise length of finite-difference cell, in.
Δy	spanwise width of finite-difference cell, in.
δ	a measure of the damping of a transient motion

θ	angle of twist in airstream direction, radians
X	dummy variable
ν	Poisson's ratio
Λ	leading-edge sweepback angle
λ	cot Λ
ρ	air density, lb sec^2 $in.^{-4}$
σ	real part of root of characteristic equation
τ	time, sec
φ	imaginary part of root of characteristic equation
Ψ	flutter parameter, $\Psi = \left(\frac{4}{\beta}\right)\left(\frac{\rho v^2}{2}\right)$
ω	angular frequency, $\omega = 2\pi f$

Subscript:

f	flutter

RESEARCH METHOD

It appears that the use of an electric-analog computer offers a practical solution to the general aeroelastic problem. The use of analog principles in representing structures has been discussed in detail in references 2 through 7. These reports show that, for examples treated, structural representation is adequate and relatively straightforward. The representation of aerodynamic forces on the analog computer has been treated in references 8 through 10. These show on the other hand that aerodynamic-force representation has in the past been rather elementary and inadequate for any but simple configurations. References 9 and 11 suggest a new approach which should be particularly satisfactory for delta wings with supersonic leading edges. It is however necessary to confirm the usefulness of such computation methods by a careful correlation between specific computations and experimental-flight or wind-tunnel tests.

In the research described in this report the physical structure of the delta wings was represented by an electrical analog for a uniform plate as described in reference 2. This analog is a complex circuit containing inductors, capacitors, and transformers. The adequacy of this representation was tested by comparing the normal modes of the analog with the known characteristics of the normal modes of the wings. The flexural rigidity of the plate was inferred from the analog rigidity required to give agreement in normal mode frequencies. This was later checked by measurements of static-influence coefficients of one wing and its analog.

Aerodynamic forces were represented in the analog by electronic transfer admittances distributed throughout the structural analog. In this way it was possible to examine the flutter characteristics for several approximate representations of the aerodynamic forces. In all cases the linearized aerodynamic theory for thin wings was used, and thickness effects were omitted.

Before presenting the results of this investigation, a short description of the flutter phenomenon and its graphical representation is given. Whether analysis is done by digital or analog methods, a continuous airfoil is almost always approximated by a system with a finite number of degrees of freedom. If the indicial lift-growth curves are approximated by a finite sum of exponential functions, then the transient response of the approximating system has a finite number of exponential time functions. These are collectively the complementary function of differential equation theory. The exponents of these time functions are the roots of the characteristic equation of the system, and for convenience are ordinarily called the roots of the system. These roots are, in general, complex numbers but because a real system is involved they must be real or must occur in complex conjugate pairs. The location of these roots determines the frequency, damping, and time constant associated with each term in the transient response. If the root in the upper half-plane is located at the point $p = \sigma + i\varphi$, then the damping is usually measured by the parameter

$$\delta = \frac{-2\sigma}{\sqrt{\sigma^2 + \varphi^2}} \tag{1}$$

A positive value of δ corresponds to a pair of roots in the left half-plane and an oscillatory transient term which dies out with time. The rate of decrement is measured by the damping factor δ. A negative value of δ corresponds to a pair of roots in the right half-plane, and a term in the complementary function which increases exponentially with time. In this case the wing is said to flutter. The damping factor may be obtained by analog or digital computational methods. It is indirectly

related to the structural parameter g used in other types of digital flutter computations, and usually shows similar but by no means identical variation.

Two methods are ordinarily used to present graphically the flutter characteristics of an airfoil. The more conventional method is a plot of either g or δ against velocity. With such a plot the frequency can be indicated by inserting numerical values of frequency at discrete points along the curve. Another method used in this report is a graphical plot of the location of the transient roots in the complex plane. Since roots appear as conjugate pairs, only the upper half of the plane is shown. These roots are continuous functions of system parameters, and if, for example, the velocity is varied, the roots trace out a continuous curve in the complex plane. When a root crosses the imaginary axis into the right half-plane, flutter occurs. In this study, the flutter parameter $\Psi = \left(\frac{4}{\beta}\right)\left(\frac{\rho v^2}{2}\right)$ is the variable used. Values of Ψ are therefore indicated by numbers placed at discrete points along the locus of a root.

PROPERTIES OF THE DELTA-WING WIND-TUNNEL MODELS

Physical Characteristics

Two delta wings were used in the experimental flutter research described in reference 1, one with leading-edge sweepback angle of 45° and the other with leading-edge sweepback angle of 60°. These will be referred to as the 45° and 60° wings for brevity. Both are cantilever semispan models made of thin magnesium sheet with leading and trailing edges beveled at an angle of 30°. Thickness ratio for the models based on mean aerodynamic chord is about .01 for both wings. Pertinent physical characteristics from reference 1 are listed in table I. The modulus of elasticity for the wing was not reported in reference 1, so a value of $E = 6.0(10)^6$ lb in.$^{-2}$ was chosen as an initial estimate.

Normal Modes of Vibration

The frequencies of the first three normal modes of vibration of each delta wing were measured in the course of the research work described in reference 1. At the same time approximate node lines were obtained for the second and third modes. Between flutter tests at different Mach numbers, the frequencies were remeasured, so that four determinations are available for each frequency. These data from reference 1, the

average values, and data from reference 12 are listed in table II(a). The node lines shown in reference 1 are reproduced in figure 1.

At a later time, the mode shapes for both wings were measured at the Langley Laboratory using a sand pattern technique. The mode shapes and frequencies for the 60° wing were provided in a private communication from the NACA flutter group at the Langley Laboratory. The mode shapes were given in the form of contour lines of constant displacement. However the results could not be compared readily with the analog-computer results, since the successive contour lines did not represent equal increments of displacement. These data were replotted in such a way that interpolation could be used to obtain comparative data. The details of this reduction are not included in this report, but the final results are shown in figure 2. Since the original data show certain inconsistencies, the mode shapes should not be assumed to be of very high accuracy.

Additional normal mode data were published in reference 12 after the flutter research described in this report had been completed. Although these data could not be used to aid in the original structural synthesis, they have since been used to confirm the accuracy of the structural representation. The data of reference 12 are again not in a form which can be directly compared with the analog results. However by cross plotting the data it is possible to construct contour lines of equal displacement as discussed above. The results of this work are also shown in figure 2. Figure 2, therefore, contains two sets of mode shapes obtained by interpolation from two different sets of data. Since the two sets of data are presumed to be the results of one physical experiment, the two sets of curves of figure 2 should be identical. The degree of correspondence observed gives a rough idea of the errors involved in the original mode shapes and in the graphical interpolation procedure used in preparation of figure 2.

Similar data for the 45° wing are shown in figure 3. In this case, the data shown became available only after the analog flutter research had been completed.

Influence Coefficients

As a result of the analog normal mode tests to be described below, it was concluded that either the mass of the wings or the assumed modulus of elasticity was in error. At the time it was assumed that the latter was in error. This was later confirmed by a measurement of influence coefficients for the 45° wing by the NACA flutter group. The influence coefficients obtained are given in figure 4. It will be noted that the matrix of coefficients shows a reasonable degree of symmetry.

Flutter Characteristics

Flutter characteristics reported in reference 1 were determined in the Langley 9- by 18-inch supersonic flutter tunnel. Tests were made at fixed Mach numbers and velocities, with air density varied to find a condition of marginal stability (incipient flutter). Both wings were tested in this way for Mach numbers equal to 1.3, 2.0, and 3.0. In addition a subsonic flutter condition was obtained in which a fixed air density was chosen, and velocity varied until flutter occurred. The experimental results presented in reference 1 are reproduced in table II(b).

STRUCTURAL PROPERTIES OF ANALOGS

Normal Modes

The methods used to represent the system by an electrical analog require replacement of the partial differential equations of a plate by finite-difference equations. The accuracy of the analog representation depends primarily upon five factors, three of which involve the actual wing, and two involve the finite-difference representation:

(a) Linearity and knowledge of the elastic properties of the cantilever-wing models

(b) Effectiveness of the cantilever-root restraint

(c) Adequacy of thin plate theory to describe the flexural properties of the cantilever-wing models

(d) Proper representation of boundary conditions at free edges, particularly along the slant leading edge

(e) The total number of finite-difference cells

With a given specific analog it is difficult, if not impossible, to separate these effects. However since inaccuracies due to items (d) and (e) should decrease as the number of cells is increased, it is possible to obtain a partial separation of items (a) through (c) from items (d) and (e) by testing analog structures with different numbers of cells. The analog computer at the California Institute of Technology can be used to represent a delta-wing cantilever plate with 21 cells. Consequently tests were made with three analogs containing 10, 15, and 21 cells as shown in figure 5. Preliminary measurements of normal mode frequencies showed that all frequencies for both 45° and 60° wings were higher than the model values by a factor of about 1.11. The specific values of this factor are given as follows:

Ratio of analog to model frequency						
Cells	45° wing			60° wing		
	Mode 1	Mode 2	Mode 3	Mode 1	Mode 2	Mode 3
21	1.098	1.115	1.121	1.096	1.088	1.101
15	1.114	1.119	1.134	1.106	1.098	1.104
10	1.133	1.152	1.157	1.124	1.122	1.124

W
1
1
2

It will be noted that the factor relating computer frequency to measured model frequency is remarkably uniform for all modes. In view of the additional close agreement between the 21- and 15-cell cases and between the 45° and 60° wing, it was believed that the major source of discrepancy lay in inadequate data regarding properties of the model.

An attempt to ascribe the discrepancy to nonrigid root restraint led to corrections which varied considerably for different modes. A root flexibility was added which was equivalent to the bending flexibility of a strip with a width 5 percent of the trailing-edge span. This was approximately eight times the wing thickness. Frequencies of the first three modes were changed by the following amounts:

Effect of root flexibility on normal modes, 15-cell case			
	Change in frequency, percent		
	Mode 1	Mode 2	Mode 3
60° wing	-6.2	-3.9	-2.7
45° wing	-6.2	-3.8	-2.2

Comparison of these numbers with the observed discrepancies shows that allowance for root flexibility will give rise to poorer consistency between analog and model results for either wing, since the first-mode frequency will be lowered more than the others. It is therefore concluded that there is no evidence for root flexibility in an amount that would significantly affect the frequencies of the normal modes.

Another factor entering into the equation of bending of a plate is Poisson's ratio ν. For a thin plate it is unlikely that reasonable variation of this ratio will affect either the mode shapes or frequencies by a significant amount. This was confirmed for the 45° wing by the use of two analog structures with ν equal to 0.25 and 0.30. Measurement

of the first four normal modes showed no significant difference in frequency and no differences in deflection that were greater than normal probable error in computer measurements. Evidently the choice of ν is unimportant for a delta wing of this thickness ratio. All subsequent work was done using the value 0.25.

Since the mass of the model is well defined and was measured, it is unlikely that there is any error in this value. The remaining specific source of error in structural properties is the estimated value of plate rigidity which depends linearly on the modulus of elasticity E and on the third power of the effective thickness t. An error of 0.0022 inch in thickness or an error of 21 percent in the estimated value of E would account for the discrepancy.

The final analog structure was obtained by decreasing the bending rigidity throughout the plate by a constant factor. The values chosen were 0.808 for the 45° wing and 0.815 for the 60° wing. These values were chosen on the basis of the 15-cell results and were made different through oversight, but since the effect of this difference on mode frequency is only 0.4 percent, the difference may safely be ignored. This change in bending rigidity corresponds to a modulus of elasticity of about $4.87(10)^6$ pound per square inch if the plate thickness is assumed to be correct. The values of model and modified analog frequencies are given in table III. Considering the scatter and evident probable error in the model data of table II, the results are in remarkable agreement.

Analog mode shapes are given in table IV for both wings represented by 10, 15, and 21 cells. In the analog structure, the displacement (but not the slope) is constrained to be zero at the inner row of cell centers. For this reason the deflections at these stations are not recorded in table IV. The stations indicated in the various cases are located at different points on the wing as shown in figure 5. For this reason it is difficult to compare mode shapes directly. However by interpolation, it is possible to represent the mode shapes by contour lines of constant deflection. This has been done for both wings, for the 15- and 21-cell cases. Results for the 60° model are shown in figure 6 and for the 45° model in figure 7. The amplitude has been adjusted so that the mode shapes for 15 cells and 21 cells correspond roughly to the same energy of excitation. In this way it is possible to see by inspection the variation in mode shape with number of cells. Even for the fourth mode the agreement is surprisingly good.

To compare these mode shapes with the three experimental modes for each model, the corresponding data for model and 21-cell analog have been plotted together in figures 8 and 9. Figure 8 contains data for the 60° wing taken from figures 2 and 6; figure 9 contains data for the 45° wing taken from figures 3 and 7. In the first mode for both wings, the contours for the analog show less curvature than the model. From an intuitive

standpoint the analog modes seem more reasonable. In the second mode the node lines are in good agreement, but with moderate discrepancies aft of the node line for the 45° wing and forward of the node line for the 60° wing. The third modes are in good agreement except near the leading edge from midspan to root. Considering the approximate nature of the experimental model modes, it is believed that the correspondence between model and analog modes is excellent and that the structure is satisfactorily represented by either the 15-cell or 21-cell analog.

Influence Coefficients

After completion of the analog flutter research described in this report, the experimental influence coefficients of figure 4 became available. Since this gave an opportunity to check the value of plate rigidity, the analog circuit for the 45° wing was set up a second time and static-influence coefficients were measured. From the measured electrical influence coefficient it is possible to infer a value for the modulus of elasticity in order to obtain a coefficient equal to the experimental value. These results are given in table V. For the 21-cell case where all four coefficients were measured and where greatest accuracy is expected, the average value for the modulus of elasticity is

$$E = 4.91 \times 10^6 \text{ lb in.}^{-2} \text{ (static-influence coefficient)}$$

This is very close to the value

$$E = 4.87 \times 10^6 \text{ lb in.}^{-2}$$

inferred from the normal-mode measurements.

The above result does not imply that the modulus of elasticity of the magnesium alloy is necessarily the value given above. Remeasurement of the 45° model thickness gave a value of 0.033 inch instead of the value of 0.034 inch reported in reference 1. If this value were used, then the value of E based on static-influence coefficients would be $5.37(10)^6$ and based on normal modes, $5.33(10)^6$ lb in.$^{-2}$. Clearly the result of tests on the analog structure can only give an inferred value of the product $E(t)^3$. The significance of the above test is that the influence coefficient measurement confirmed the value of plate rigidity required to duplicate the normal-mode frequencies with discrepancy less than 1 percent.

REPRESENTATION OF AERODYNAMIC FORCES

Aerodynamic forces on a delta wing can be approximated in many different ways. In this section consideration will be given to some of the methods suitable for supersonic speeds when the leading edge is supersonic. It is well known that the two-dimensional steady-state lift coefficient for a thin airfoil with rigid chord is $4/\beta$ and that the pressure over the airfoil is constant from leading edge to trailing edge. For a rigid unswept finite wing with constant chord the same result holds except near the tip where for a spanwise distance of c/β a portion of the flow is mixed subsonic-supersonic. On a rigid delta wing the pressure distribution is somewhat different. For the case of a supersonic leading edge the wing can be divided into two regions by the Mach cone sweeping aft from the apex of the wing. Outside the cone the pressure is constant and is larger than the value based on the two-dimensional lift coefficient, $4/\beta$. Inside the Mach cone the pressure varies in the manner shown in figure 10. However the overall or average lift coefficient for the wing has a theoretical value precisely equal to $4/\beta$, no matter what the speed or Mach number. Inspection of figure 10 shows that as the Mach number increases the steady-state pressure distribution on a rigid delta wing is more nearly constant and the "local" lift coefficient more nearly approaches the constant value $4/\beta$. Needless to say, the pressure distribution is modified for motion which differs from that of a rigid wing.

The above considerations suggest that a relatively crude approximation to the aerodynamic forces is the simple assumption that the pressure everywhere depends upon the local downwash or angle of attack and that there is no lag in the development of this pressure:

$$p = \left(\frac{\rho v^2}{2}\right)\left(\frac{4}{\beta}\right)\alpha \qquad (2)$$

where

$$\alpha = \left(\dot{h} + \frac{\theta}{v}\right)$$

However, it is clear that at low Mach numbers and for other than rigid wing mode shapes this assumption may lead to large errors.

Another representation which is well adapted to the methods of conventional flutter analysis is a simple strip theory. For such an approximation, the delta wing is divided into strips parallel to the airstream and lumped aerodynamic forces are applied to these strips. In its simplest form, camber is neglected and the aerodynamic force and

moment are assumed to depend only upon the motion (angle of attack and pitch) of the section for which the force is to be computed. This method may be extended in complexity by the following additional features:

(a) The forces on a specified strip may be given a dependence upon the motion of adjacent strips.

(b) Lift and moment forces due to camber may be included. The simplest assumption is that of constant curvature or "parabolic camber." A more complex representation is required if cubic or "S" shaped camber is significant.

(c) Camber forces or chordwise bending moments may be represented.

The degree of complexity which is justifiable in an engineering sense is greatly limited by the fact that the details of representations (a), (b), and (c) above have only been partially worked out in a form suitable for computation. Omitting these features the aerodynamic forces on the ith strip can be approximated by the equations:

$$F_i = \left(\frac{\rho v^2}{2}\right)\left(S_i\right)\left\{C_{L_\alpha}(\tau) * \alpha_{x_1}(\tau)\right\} \tag{3}$$

$$M_i = \left(\frac{\rho v^2}{2}\right)\left(S_i c\right)\left\{C_{M_q}(\tau) * q(\tau)\right\} \tag{4}$$

The approximations involved in these equations are discussed in appendix A.

Another possibly more accurate representation is obtained through use of equation (15a) of reference 13. The linearity of this equation shows that the pressure at any point can be obtained by an integration of the downwash or angle of attack over the surface of the wing.

$$p_j = \left(\frac{\rho v^2}{2}\right)\iint_S \left\{k\left[\left(x_j - x_i\right),\left(y_j - y_i\right),\tau\right] * \alpha_i(\tau)\right\} dS_i \tag{5}$$

This in turn implies that the pressure may be approximated to any required degree of accuracy by a summation, the elements of which are obtained by dividing the wing into small areas and multiplying each area by the convolution of an influence coefficient and an average local angle of attack.

$$F_j = p_j \Delta S_j = \left(\frac{\rho v^2}{2}\right) \sum_j \left\{ k_{ij}(\tau) * \alpha_i(\tau) \right\} \Delta S_j \qquad (6)$$

Omitting the time dependence of k_{ij}, or in other words assuming the indicial response is a step function, equation (6) takes on the simple form

$$F_j = \frac{\rho v^2}{2} \sum_i k_{ij} \alpha_i \Delta S_j \qquad (7)$$

W
1
1
2

where k_{ij} is a coefficient which depends only on geometry and Mach number. This equation is valid for steady-state motion and for slowly varying time-dependent motion. When time dependence is important, evaluation of $k_{ij}(\tau)$ is difficult. For flutter computations, interest is primarily centered on the case of incipient flutter in which case steady-state sinusoidal motion prevails. If such oscillatory motion is assumed, it is possible to calculate the steady-state pressure (magnitude and phase angle) as a power series in frequency. This power series can be used to synthesize electrical circuits which will give good accuracy for low-frequency sinusoidal motion, and a reasonable approximation to the force for arbitrary motion. Methods of dividing the wing into cells and evaluating the coefficients k_{ij} are discussed in appendix B.

Equations (6) and (7) show that the actual velocity enters into flutter computations at two points, first in the determination of the dynamic pressure $\frac{\rho v^2}{2}$ and second in determination of the downwash

$$\frac{w}{v} = \alpha = \theta + \frac{\dot{h}}{v} \qquad (8)$$

In the results which follow it will be found that in the second instance the effect is of second order, so that the experimental value of velocity may be used in the computation of α with negligible error. On the other hand, if the pressure distribution is determined by Mach number and mode shape, then the result of a flutter computation is not flutter velocity but a value of $\frac{\rho v^2}{2}$, the dynamic pressure, at which marginal stability results.

Another important parameter is the dynamic pressure multiplied by the two-dimensional lift coefficient. This is defined in this report as the flutter parameter and indicated by the symbol Ψ.

$$\Psi = \left(\frac{4}{\beta}\right)\left(\frac{\rho v^2}{2}\right) \tag{9}$$

In reporting results of flutter computations, values of $\frac{\rho v^2}{2}$ and Ψ will be given rather than a density based on the experimental value of v or a velocity based on the experimental value of ρ.

ANALOG COMPUTER FLUTTER COMPUTATIONS

Strip Theory

For wing motion in which there is little wing camber and at high Mach numbers, strip theory can be applied. For Mach numbers high enough, there is negligible lag in the growth of aerodynamic lift due to angle of attack, and for properly chosen reference axes the only important aerodynamic terms are C_{L_α} and C_{M_q}, the other terms C_{L_q} and C_{M_α} being effectively zero. As stated in appendix A, the choice of midchord for reference axis is probably most suitable for a delta wing at high Mach numbers, although near the root the center of pressure x_o moves slightly forward. Aerodynamic forces as described by equations (3) and (4) can be very readily represented on the analog computer, affording an easy means of comparing strip theory computations with box theory for delta wings.

Using the aerodynamic coefficients

$$C_{L_\alpha} = 4/\beta$$

$$C_{L_q} = 0$$

$$C_{M_\alpha} = 0$$

$$C_{M_q} = 1/3\beta$$

$$x_o = x_1 = 0.50$$

$$C_{L_\alpha}(\tau) = C_{L_\alpha}$$

flutter analysis was carried out for the 45° wing and the 60° wing at Mach numbers of 2.0 and 3.0. The 15-cell structure was used, with one aerodynamic "cell" or strip associated with each chordwise row of structural cells. There were therefore 15-structural cells and 5 aerodynamic strips although the root strip, having negligible motion and being nearest the cantilever restraint, was omitted. The outer four strips were represented aerodynamically, with lift force applied at the appropriate point $x_o c$ behind the leading edge, where c is the local chord. This force was calculated using the downwash at a point a distance $x_1 c$ behind the leading edge

$$\alpha = \frac{w}{v} = \theta + \frac{\dot{h}_{x_1}}{v} \tag{10}$$

For convenience, the angle θ was measured at the midchord since θ does not vary greatly with chordwise position and since x_1 does not vary greatly from the value 0.50.

The results given in table VI are significantly different from the wind-tunnel data and the results for box theory. In the first place, the values of $\frac{\rho v^2}{2}$ are considerably lower than experimental values, although as might be expected the agreement is better at high Mach numbers and for the 45° wing. In the second place, the computed flutter frequency is considerably below the experimental value, 20 percent for the 45° wing and over 30 percent for the 60° wing. It is also of interest to note that the analog results show no trend of the flutter parameter Ψ with Mach number although the experimental data does.

As part of the investigation of strip theory, an effort was made to obtain better agreement through variation of the important aerodynamic parameters. The principal variations to be considered are in the steady-state values of the coefficients C_{L_α} and C_{M_q}, the locations of the reference axes x_o and x_1, and the time variation of the indicial lift coefficient $C_{L_\alpha}(\tau)$. As long as the parameter C_{L_α} is maintained constant across the span, variation in the steady-state value of C_{L_α} results only in a change in the parameter $\frac{\rho v^2}{2}$ without any change in the flutter frequency. The change in C_{L_α} required to reach agreement with experiment is listed as follows:

	45° wing		60° wing	
Mach number	2.0	3.0	2.0	3.0
Increase in C_{L_α}, percent	19	10	64	31

There does not seem to be a simple justification for these changes and since flutter frequency is not affected, the discrepancy in frequency remains large.

The next factor varied was the parameter C_{M_q}. To demonstrate its small effect, this term was set equal to zero with results shown in table VI. The percentage change in $\frac{\rho v^2}{2}$ was remarkably small considering the fact that the term was not reduced by a small factor but removed entirely. Evidently this coefficient cannot be modified to give agreement with experiment.

A third important aeroelastic parameter is the center of pressure x_o. For constant angle of attack the value of x_o is 0.50 referred to the local chord in the outer regions of the wing. Near the root the center of pressure is theoretically forward of the midchord except at the root where the center of pressure is again at the midchord. At high Mach numbers $\beta\lambda \gg 1$ this effect is quite small with center of pressure near the midchord at all span positions. On the other hand, for a linear or parabolic bending mode shape the value of x_o is more likely to be about 0.70 near the root and perhaps 0.40 near the tip, the actual value depending somewhat, but not critically, on the actual mode shape and the effective aspect ratio $A' = A\beta$. The importance of this term was investigated by varying x_o separately at each strip with results shown in table VII(a). It can be seen that moving the center of pressure forward at the tip increased the discrepancy both in $\frac{\rho v^2}{2}$ and f_f. Near the root moving the center of pressure aft gives better agreement but the overall effect is small. If, for example, one chooses the values

Strip	0 (root)	1	2	3	4 (tip)
x_o	0.70	0.60	0.55	0.50	0.45

then the overall change in $\frac{\rho v^2}{2}$ for the 60° wing is about 2 percent and the net change in flutter frequency is 2 cps. Evidently a reasonable variation in x_o will not provide agreement with experimental results.

The two remaining aerodynamic parameters of importance are the time variation of indicial lift coefficient $\frac{C_{L_\alpha}(\tau)}{C_{L_\alpha}(\infty)}$ and the rotation center location x_1. The first of these was observed to have such small effect that the data were not included in this report. The second was also found to be relatively unimportant. The results shown in table VII(b) indicate the location of rotation center x_1 to be less important than the location of moment center x_o by a factor greater than 10.

The final conclusion is that simple strip theory cannot be used or even modified to give good agreement with experimental data. It appears that "camber" or "flap" forces and interactions between adjacent strips must be represented if this approach is to be used. On the other hand, the introduction of leading- and trailing-edge flaps effectively triples the number of aerodynamic interactions which makes it comparable in complexity to the box method which is somewhat easier to use. No computations of this type were attempted.

Box Method

Flutter computations using the box method were made with several simplifying assumptions regarding the nature of the aerodynamic forces. These are described in appendix B.

Case A.- In case A it is assumed that the pressure at a point depends only upon the local motion with lift coefficient equal to the two-dimensional value. Aerodynamic forces of this nature would give a flutter frequency and flutter mode shape independent of Mach number, and a constant value for the flutter parameter Ψ. It is possible to examine the data of reference 1 for consistency with this assumption. Table VIII lists the computed value of flutter frequency, dynamic pressure $\frac{\rho v^2}{2}$, and the aerodynamic parameter Ψ. To facilitate comparison the ratio of computed and experimental values of Ψ are also tabulated. Data for the 45° wing show reasonable constancy, with variation in Ψ of about 14 percent between Mach numbers of 1.5 and 3.0. However the 60° wing shows a 22-percent variation between Mach numbers 2.0 and 3.0. At best this aerodynamic assumption would be expected to predict flutter conditions with accuracy in the parameter Ψ of perhaps 20 or 30 percent.

There are three outstanding features to be noted in case A of table VIII. First, the agreement between observed and computed values is surprisingly good for such a simple representation of aerodynamic forces. Second, the lack of agreement, though not large, shows a significant and regular trend. Although the experimental values of $\overline{\nu}$ vary with Mach number, the computed values are essentially constant. This result is the justification for the remark made earlier that the velocity term in the downwash equation has only a second-order effect on the flutter condition. It will also be noted that the agreement with experiment is best at low Mach numbers. This result is contrary to expectation since the aerodynamic-force representation should deteriorate at low Mach numbers. It is probable that there are other compensating sources of error, such as oversimplification of pressure distribution. The third feature to be noted is that there is very little difference between the 10-, 15-, and 21-cell representations. This is quite surprising since the 10-cell case has aerodynamic forces represented at only six stations on the wing (cells 1 to 6 in fig. 5), as compared with fifteen stations for the 21-cell case.

Case B.- A more accurate approach is one which correctly ascribes the force at a station to the motion of that portion of the wing located within the forward sweeping Mach cone. This can be done approximately by the methods discussed in references 9 and 13. This approach does not require any prior knowledge of the flutter mode shape, but is necessarily more complicated than case A because of the aerodynamic interactions allowed between various parts of the wing surface. For this investigation it was first assumed that the transit time of all interaction effects was small. Aerodynamic forces were therefore approximated using equation (7). The values of k_{ij} were calculated using equations in appendix B and are listed in table IX.

The results are presented in case B of table VIII. Comparison with case A shows that this assumption results in much better agreement with the experimental data. There is however still a moderate discrepancy at the highest Mach number for both wings.

Case C.- As described earlier, each aerodynamic influence coefficient can be described by a power series expansion in frequency. Equations for the first three terms are given in appendix B and numerical values are listed in table IX. For the frequencies encountered in this problem only two or three terms are required to insure errors far less than 1 percent. In fact, inspection of the coefficients would lead one to expect very little difference between use of the complete power series and use of only the constant (zero frequency) term, case B.

Results for a representation accurate to the first power in frequency are given in case C of table VIII. As expected the difference between this case and case B is slight. The effect is greatest with the

45° wing at Mach number 1.5 where the computed parameter $\frac{\rho v^2}{2}$ changes by about 2.5 percent. At Mach number 2.0 the effect is only 1 percent, indicating similar computations at Mach number 3.0 unnecessary. Similarly with the 60° wing the effect is greatest at the lower Mach numbers. However, even at the lowest value, Mach 2.0, the effect was a reduction of only 3 percent in the parameter $\frac{\rho v^2}{2}$. At Mach 3.0 the reduction was about 1 percent. It appears that any further refinement to bring about better agreement between computation and wind-tunnel results must involve a refinement of the static- (zero frequency) pressure coefficients for an arbitrarily deformed wing.

W
1
1
2

Effect of Individual Pressure Interactions

Aerodynamic pressures at various points on the wing undoubtedly have varying effect in producing flutter. To determine the location of the more critical areas on the wing, all pressure interactions were varied one at a time for the case of 45° wing, 15-cell structure, Mach 2.0. An individual pressure interaction on the jth cell was denoted by

$$p_{ij} = \left(\frac{\rho v^2}{2}\right)\left(k_{ij}\right)\alpha_i \, \Delta S_j \tag{11}$$

The effect of a change in p_{ij} can be expressed as a change in $\frac{\rho v^2}{2}$ for flutter per unit change in the coefficient k_{ij}. Expressed this way the effect can be described numerically by the parameter

$$k_l = \frac{\left[\Delta \frac{\rho v^2}{2} \Big/ \frac{\rho v^2}{2}\right]}{\left[\Delta k_{ij} / k_{ij}\right]} \tag{12}$$

Table X lists the values of k_l for all interacting cells for the 45° wing, Mach 2.0, 15-cell case.

These results are significant but a little difficult to interpret because the effect of a given interaction depends upon three factors:

(a) Angle of attack at the ith cell

(b) Magnitude of the interaction coefficient k_{ij}

(c) Effectiveness of a force on the jth cell in inducing flutter

It is the third of these factors that is desired here. This information can be obtained from another coefficient k_2 defined below.

$$k_2 = \frac{k_1 k_{jj}}{\alpha_i k_{ij}} \tag{13}$$

If the wing is moving so that all of the α_i are in phase, then all values k_2 for a given j should be equal and the values of k_2 for different j provide a relative measure of the desired factor. For computing k_2, values of α_i were measured at flutter. It was noted that the various values were not exactly in phase particularly near the root and forward on the wing, so that close agreement in the values of k_2 for a given value of j is not to be expected. Values of this factor are also given in table X and do show the anticipated results. A negative value of k_2 implies that $\frac{\rho v^2}{2}$ is smaller if k_{ij} is increased, that is, flutter occurs at a lower value of $\frac{\rho v^2}{2}$. It can be seen that forces along the leading edge are the ones that contribute to the onset of flutter, whereas forces along the trailing edge have a stabilizing effect.

This would seem to be equivalent to a statement that moving the center of pressure forward at any station should have a destabilizing effect. The possible equivalence of these statements will be discussed in the next section.

Location of Center of Pressure

Shifting the center of pressure of various cells was investigated for several configurations including all three Mach numbers, case A and case B. Results were remarkably uniform so the data for only case A at Mach 3.0 will be presented. Table XI lists the per unit change in $\frac{\rho v^2}{2}$ per unit shift of center of pressure for each cell. For example, if the center of pressure of cell 3 is shifted forward 1 percent of the cell length (a distance equal to 0.5 percent of the local chord), the computed

value of $\frac{\rho v^2}{2}$ is decreased approximately 1.8 percent. This result is consistent with the results of the preceding section. It can be seen from table XI that the effect is greatest for the outer parts of the wing, but the effect is still significant at the 40-percent span position.

The results of the last two sections suggest that simple variation in the magnitude-of-pressure interactions or the centers of pressure can be used to explain the discrepancies observed for the cases B and C. As yet no logical procedure has been found for achieving this result. For example, it seems plausible that the pressure interactions and centers of pressure should be least accurate at low Mach numbers, yet for these cases the basic results are the most accurate.

Flutter Mode Shape

Some insight into the flutter problem is afforded by consideration of the flutter mode shape. Experimentally it is found that the calculated flutter mode shape does not depend significantly upon the various assumptions considered for aerodynamic representation. Approximate mode shapes were measured with the analog computer for the 15-cell representation of both wings at Mach number of 3.0. These mode shapes are given in table XII. It can be seen that the mode shape is similar to the first vibration mode of the wing, although the frequency is about three times as great.

DIGITAL CHECKS

Analog computation, as all computation, requires a careful checking procedure to insure accuracy of the results. A part of the established procedure involves digital checks on various simplifications of the system. For example, the simplest representation of aerodynamic forces, case A, can be used with two or three of the normal modes to obtain an approximate behavior of the system. To pass from this aerodynamic representation to any of the more elaborate ones may involve great complication of the digital procedure, but it requires a negligible extension of analog procedure. Thus a digital check of the simpler system can be used to assure that the analog circuit is set up properly not only for the simple system but for the more complex aerodynamic representation as well. In addition, a digital check of this type gives additional information regarding the normal modes primarily involved in flutter and gives a flutter mode shape as a linear combination of the normal modes. The analog computer gives the flutter mode shape directly, but it does not relate it to the normal modes. For these reasons, a series of digital checks have been made. In all cases the normal modes of the 15-cell structure were used, and

the aerodynamic force at each cell was made proportional to the local downwash:

$$F_i = \left(\frac{\rho v^2}{2}\right)\left(\frac{4}{\beta}\right)\left(\Delta S_i\right)(\alpha_i) \tag{14}$$

Except where otherwise noted the quantity α was calculated from the relation

$$\alpha = \left(\theta + \frac{\dot{h}}{v}\right) \tag{15}$$

As mentioned earlier the term $\dot{h}/v$ in equation (15) is of secondary importance, with flutter characteristics dependent almost entirely on the value and possible spanwise and chordwise variation in lift coefficient.

Flutter Analysis Using Two Modes

Inspection of normal-mode shapes in figures 2 and 3 shows that the first mode is predominantly a bending mode, the second mode predominantly torsion, while the third mode shows characteristics of a second bending mode with some torsion. In view of the observed value of flutter frequency, it is to be expected that flutter will primarily involve the two lowest modes.

A computation was made using these modes for both 45° and 60° wings at Mach numbers equal to 2.0 and 3.0. The computed values of Ψ and flutter frequency f_f are given in table XIII. Also included are wind-tunnel and analog-computer values. Comparison of the data leads to the following conclusions.

(a) The first two normal modes play a dominant role in producing flutter of these wings.

(b) The essentially constant value of Ψ does not agree with the experimental trend where Ψ decreases as Mach number increases, particularly for the 60° wing.

(c) The difference between computations at two Mach numbers lies only in the value of v in equation (15). Between Mach 2.0 and Mach 3.0, this value changes 20 percent. Since this changes the value of Ψ only 1 or 2 percent, it is clear that the precise value of v used in equation (15) does not significantly affect the flutter condition even though it is the major source of aerodynamic damping in the system.

(d) It seems reasonable that the simplified aerodynamics would give the most accurate agreement with experimental results at high Mach numbers. This expectation is contrary to the results for the 60° wing. At Mach number of 2.0 for the 60° wing, and for both Mach numbers for the 45° wing, the calculated values of Ψ are very close to the experimental values.

(e) Calculated flutter frequencies are lower than the experimental values.

W
1
1
2

Three and Four Mode Flutter Analysis

In order to investigate the discrepancies in items (d) and (e) of the preceding section, similar computations were made using the first three modes for both the 45° and 60° wing, and using four modes for the 45° wing. These results, also included in table XIII, confirm the first two conclusions above and modify the last two as follows:

(d) The close agreement in the parameter Ψ for certain cases was fortuitous and not significant for the two mode case. The values obtained using more modes are definitely higher, and in good agreement with the analog computer which utilizes, or more correctly represents, even more of the modes.

(e) The calculated flutter frequency shows better agreement with experiment when more modes are used.

In addition, the following data can be obtained regarding the flutter mode shape. Using the lowest two modes as given for the 15-cell structure in table IV, the flutter mode shape consists of 86 percent first mode and 14 percent second mode. Using the lowest three modes the percentages are 84 percent first mode, 14 percent second mode and 2 percent third mode. It is clear that flutter involves primarily the lowest two modes.

Two Mode Analysis With Structural Damping

As a result of some paradoxical analog results, four complete digital checks were made using two modes. These checks included computation of the location of the four roots of the system for values of Ψ ranging from zero (no aerodynamic forces) to a value well above flutter. Two of the cases do not show a well defined flutter, so that it is more informative to plot the actual system-root locations as functions of Ψ rather than to merely list the flutter condition for each case. The four cases considered here are the flutter computations for the 45° wing using two modes and various assumptions regarding aerodynamic forces and structural

damping of the two modes, g_1 and g_2. The modes used in these computations are the first two normal modes of the 15-cell analog.

Case	Aerodynamic force	g_1	g_2
1	$P_j = \Psi \Delta S_j(\theta_j)$	0	0
2	$P_j = \Psi \Delta S_j(\theta_j)$	0.05	0.03
3	$P_j = \Psi \Delta S_j\left(\theta + \frac{\dot{h}}{v}\right)_j$	0	0
4	$P_j = \Psi \Delta S_j\left(\theta + \frac{\dot{h}}{v}\right)_j$	0.05	0.03

In case 1 there is no source of damping in either the structure or the aerodynamic forces. As a result, for Ψ increasing from zero, the roots are constrained to move along the imaginary axis starting at points in the complex plane corresponding to the two-structural normal modes. Since the roots move in opposite directions from the starting points, they must meet at some particular value of Ψ and then split, one moving into the left half-plane, the other into the right half-plane. Inspection of the equations of the system shows that the characteristic equation contains only even powers in the variable which determines root location. Consequently the plot of the roots must show complete quadrantal symmetry as shown in figure 11(a). Below $\Psi = 14.6$ the damping associated with all roots is zero, but one cannot properly say that a flutter condition exists. However, for larger values a definite flutter occurs. In comparing with the other cases it seems consistent to say that flutter occurs at a frequency of 150 cps ($\omega = 940$) when Ψ is equal to 14.6.

It is to be expected that structural damping will move the roots over into the left half-plane, at least for small values of Ψ. In case 2, the values chosen for structural damping are the inherent damping measured in the analog circuit, and are perhaps slightly larger than the values for the model. The results shown in figure 11(b) are only slightly different from the results for case 1. This was one of the cases regarded as paradoxical when first studied with the analog computer. The results obtained with the analog computer are compared with the digital results in figure 12. On the basis of data given earlier, it is expected that the analog system will show a root bending into the right half-plane at a higher frequency than the two mode system and at a higher value of Ψ. Figure 12 shows that this is indeed the case. The correspondence between the two systems is considered satisfactory.

In case 3 with the downwash properly represented, the roots move more definitely into the left half-plane, and show a more definite flutter at a frequency of 150.5 cps and a Ψ value of 14.9. These values are listed in table XIII and were referred to earlier. The entire locus of roots is shown in figure 11(c).

Case 3 represents the basic check case except that the analog computer has the small amount of inherent structural damping used in case 2. A digital solution (fig. 11(d)) including structural damping is provided by case 4. Evidently, the flutter condition is not significantly changed, with f_f = 149 cps and Ψ = 15.0. Since structural damping has a negligible effect on this system, it is expected that it would have a corresponding small effect on flutter condition for the actual wing.

W-1122

CONCLUSIONS

At supersonic speeds the flutter of simple delta wings of the type examined is a phenomenon involving primarily the two lowest normal modes of the wing. Use of more than the three or four lowest modes in flutter analysis does not give a significant improvement in accuracy. Greatest accuracy in supersonic flutter computations was obtained using the box method, with the pressure at a given point dependent upon the motion of that point and all other points within the forward sweeping Mach cone. Flutter for both 45° and 60° wings was predicted with good accuracy at low Mach numbers but at the highest Mach number (Mach 3.0) there was a significant discrepancy in the experimental and computed values of dynamic pressure $\frac{\rho v^2}{2}$ at flutter. This discrepancy was equivalent to a 20-percent error in density for the 45° wing and a 35-percent error for the 60° wing, or alternatively was equivalent to a 10-percent error in velocity for the 45° wing and a 16-percent error for the 60° wing. Judging from the trends of Ψ with number of cells, this would be somewhat improved by using a larger number of cells. However it does not appear that the large discrepancy at Mach 3.0 would be eliminated by use of any number of cells.

For the wings considered, any lag in the development of aerodynamic lift was completely negligible from the standpoint of influence on flutter. It is also to be noted that the computed flutter conditions are in general unconservative, indicating a value of $\frac{\rho v^2}{2}$ greater than the experimental value. However the degree of unconservativeness is not significant except at the highest Mach numbers.

A possible explanation of the discrepancy lies in the effect of wing thickness which should become larger at the higher Mach numbers. A preliminary estimate indicates that over the beveled leading edge, the local lift coefficient is increased by a factor of 4 or 5 at Mach 3.0, while at the trailing edge it may be increased by a factor of 2. Although the area involved is small, it is to be noted in tables X and XI that an increased lift coefficient at the leading edge would have the greatest effect on the flutter condition. Using the numbers above and values of k_1 from table IX it can be shown that the computed value of $\frac{\rho v^2}{2}$ would be reduced by about 20 percent for the 45° wing at Mach 3.0. Because of lack of data, similar estimates cannot be made for the 60° wing but presumably the effect would be similar.

California Institute of Technology,
Pasadena, Calif., March 14, 1958.

APPENDIX A

STRIP THEORY APPROXIMATION TO AERODYNAMIC FORCES

When camber is negligible, two-dimensional aerodynamic forces can be completely specified by four coefficients

$$F = \left(\frac{\rho v^2}{2}\right)(S)\left[\left\{C_{L_\alpha}(\tau)*\alpha(\tau)\right\} + \left\{C_{L_q}(\tau)*q(\tau)\right\}\right] \tag{16}$$

$$M = \left(\frac{\rho v^2}{2}\right)(cS)\left[\left\{C_{M_\alpha}(\tau)*\alpha(\tau)\right\} + \left\{C_{M_q}(\tau)*q(\tau)\right\}\right] \tag{17}$$

When moment reference axis x_o and rotation center x_1 are properly chosen, the steady-state values of C_{L_q} and C_{M_α} are zero and the overall contributions of these terms are small for conventional flutter involving simple bending and torsion with bending frequency well below torsion frequency. Omitting these terms, the equations above reduce to equations (3) and (4). A method frequently used for flutter analysis of finite wings is to represent the local forces by these equations but in which the brackets are taken to be matrices, thus allowing aerodynamic interactions between strips on the wing. This method should give satisfactory results whenever forces due to camber are negligible. For high supersonic speeds the matrices are largely diagonal and the time variation of the coefficients is small. In this case equations (3) and (4) can be interpreted as simple scalar equations giving the local forces in terms of the local motion.

$$F_i = \left(\frac{\rho v^2}{2}\right)\left(S_i\right)\left(C_{L_\alpha}\left[\alpha_{x_1}(\tau)\right]\right. \tag{18}$$

$$M_i = \left(\frac{\rho v^2}{2}\right)\left(S_i c\right)\left(C_{M_q}\ \left[q(\tau)\right]\right. \tag{19}$$

where

$$\alpha_{x_1} = \theta + \frac{h_{x_1}}{v}$$

$$q = \frac{c}{v}\,\dot{\theta}$$

The choice of local value of x_o is usually made so that the load distribution is approximately correct for a deflection shape similar to the expected flutter mode shape. The value of x_1 is usually taken to be $(1 - x_o)$ although as shown in this report the effect of its variation from this value is quite insignificant. These matters are discussed critically in reference 10.

For the present study, the preliminary values of the important aerodynamic parameters were taken to have the values:

$$C_{L_\alpha} = \frac{4}{\beta}$$

$$C_{L_q} = 0$$

$$C_{M_\alpha} = 0$$

$$C_{M_q} = \frac{1}{3}\beta$$

$$x_o = x_1 = 0.50$$

$$C_{L_\alpha}(\tau) = C_{L_\alpha}$$

However, in the course of the investigation all of these were varied.

APPENDIX B

BOX THEORY APPROXIMATION TO AERODYNAMIC FORCES

It is assumed that the downwash is constant over the area of a box so that the pressure interaction between a given box and another can be evaluated, using equations (17) and (19) of reference 13, with the integration of equation (19) restricted to the area of the interacting box rather than the entire area inside the Mach cone. Since the integral indicated in equation (19) cannot be written in closed form using known functions, it is simplest to expand the cosine and exponential functions in a power series in frequency and integrate term by term. Using the relative coordinates shown in figure 13, the pressure at the center of the jth cell due to uniform motion of the ith cell can be written

$$p_{ij} = -\left(\frac{\rho v^2}{2}\right)\left(\frac{4}{\beta}\right)\left(\frac{w_i e^{i\omega\tau}}{v}\right)\left[P_0 + i\left(\frac{\omega}{c\beta^2}\right)P_1 + \left(\frac{\omega}{c\beta^2}\right)^2 P_2 + i\left(\frac{\omega}{c\beta^2}\right)^3 P_3 + \cdots\right] \tag{20}$$

where

$$P_0 = \frac{1}{\pi}\left[\cos^{-1}\frac{\beta\zeta_1}{\xi_2} + \cos^{-1}\frac{\beta\zeta_2}{\xi_1} - \cos^{-1}\frac{\beta\zeta_1}{\xi_1} - \cos^{-1}\frac{\beta\zeta_2}{\xi_2}\right] \tag{21}$$

$$P_1 = -\frac{1}{M\alpha\pi}\left\{\xi_2\left(\cos^{-1}\frac{\beta\zeta_1}{\xi_2} - \cos^{-1}\frac{\beta\zeta_2}{\xi_2}\right) - \xi_1\left(\cos^{-1}\frac{\beta\zeta_1}{\xi_1} - \cos^{-1}\frac{\beta\zeta_2}{\xi_1}\right) + \beta^2(\beta\zeta_1)\left(\cosh^{-1}\left|\frac{\xi_2}{\beta\zeta_1}\right| - \cosh^{-1}\left|\frac{\xi_1}{\beta\zeta_1}\right|\right) - \beta^2(\beta\zeta_2)\left(\cosh^{-1}\left|\frac{\xi_2}{\beta\zeta_2}\right| - \cosh^{-1}\left|\frac{\xi_1}{\beta\zeta_2}\right|\right)\right\} \tag{22}$$

$$P_2 = -\frac{1}{2\pi}\left\{\frac{3}{2}\xi_2^2\left[\cos^{-1}\frac{\beta\zeta_1}{\xi_2} - \cos^{-1}\frac{\beta\zeta_2}{\xi_2}\right] - \frac{3}{2}\xi_1^2\left[\cos^{-1}\frac{\beta\zeta_1}{\xi_1}\cos^{-1}\frac{\beta\zeta_2}{\xi_1}\right] + \right.$$

$$\beta^2\left(Ma^2 - \frac{3}{2}\right)\zeta_1\left[\sqrt{\xi_2^2 - \beta^2\zeta_1^2} - \sqrt{\xi_1^2 - \beta^2\zeta_1^2}\right] -$$

$$\left.\beta^2\left(Ma^2 - \frac{3}{2}\right)\zeta_2\left[\sqrt{\xi_2^2 - \beta^2\zeta_2^2} - \sqrt{\xi_1^2 - \beta^2\zeta_2^2}\right]\right\} \qquad (23)$$

W
1
1
2

and where w is given by equation (8). Evidently the function k_{ij} defined in the text is represented by the product of $4/\beta$ and the power series within the brackets. When one or more of the corners of a rectangle lie outside the Mach cone, some of the functions in these equations are undefined. It can be shown that the results are correct if the following convention is adopted.

$$\cos^{-1}\frac{\beta\zeta}{\xi} = 0 \quad \text{if} \quad \frac{\beta\zeta}{\xi} > 1$$

$$\cos^{-1}\frac{\beta\zeta}{\xi} = \pi \quad \text{if} \quad \frac{\beta\zeta}{\xi} < -1$$

$$\cosh^{-1}\frac{\xi}{\beta\zeta} = 0 \quad \text{if} \quad \left|\frac{\xi}{\beta\zeta}\right| < 1$$

$$\sqrt{\xi^2 - \beta^2\zeta^2} = 0 \quad \text{if} \quad \frac{\beta\zeta}{\xi} > 1$$

Functions of the form of equations (21) to (23) could be integrated over the jth cell to get the total force on this cell. However it appears that sufficient accuracy results if the pressure at the center is simply multiplied by the area of the jth cell. Additional inaccuracy results when the ith cell lies along the leading edge of the delta wing. It is possible to use the true shape of the wing here and represent the slant leading edge, but preliminary attempts to do this led to unusual difficulties and to both poor and inconclusive results. The results of this investigation are not contained in this report; in any case the

discrepancies have not been resolved. The coefficients P_0 and P_1 used in this study are tabulated in table IX.

In this investigation, several assumptions were used for approximating the aerodynamic forces. Three of these are discussed in this report. In case A, the pressure was assumed to depend only upon the local motion, with no time dependence. That is, only the coefficient P_0 for $(i = j)$ was used in equation (20). All other coefficients were taken to be zero. In case B the steady state pressure was ascribed to the wing deflections in the forward sweeping Mach cone, but no time dependence was assumed. In this case all of the P_0 coefficients in table IX were used, with coefficients P_1, P_2, . . . etc. taken to be zero.

W
1
1
2

Case C differed from case B in that the P_1 coefficients were properly represented. The higher order coefficients though automatically present by virtue of the computation method used, were not necessarily equal to the correct value. It was not felt necessary to match the frequency response beyond the first power because of the insignificant effect of the higher order terms.

REFERENCES

1. Tuovila, W. J., and McCarty, John Locke: Experimental Flutter Results for Cantilever-Wing Models at Mach Numbers Up to 3.0. NACA RM L55E11, 1955.

2. MacNeal, Richard H.: The Solution of Partial Differential Equations by Means of Electrical Networks. Ph.D. Thesis, C.I.T., 1949.

3. Benscoter, Stanley U., and MacNeal, Richard H.: Introduction to Electrical-Circuit Analogies for Beam Analysis. NACA TN 2785, 1952.

4. Benscoter, Stanley U., and MacNeal, Richard H.: Equivalent Plate Theory for a Straight Multicell Wing. NACA TN 2786, 1952.

5. McCann, G. D., and MacNeal, R. H.: General Methods of Synthesis for Electrical-Mechanical Analogies of Aircraft Structures. ARDC Tech. Rep. No. 1, Contract AF-18(600)-669, Oct. 1954.

6. MacNeal, R. H.: Vibrations of Composite Systems. ARDC Tech. Rep. No. 1, Contract AF-18(600)-669, Oct. 1954.

7. MacNeal R. H.: The Equivalent Circuits of Shells Used in Airframe Construction. Proc. Joint IRE, AIEE, ACM Western Computer Conf., 1953.

8. MacNeal, R. H., McCann, G. D., and Wilts, C. H.: The Solution of Aeroelastic Problems by Means of Electrical Analogies. Jour. Aero. Sci., vol. 18, no. 12, Dec. 1951, pp. 777-789.

9. Basin, Machael Abram: Electric Analog Computer Study of Supersonic Flutter of Elastic Delta Wings. Ph.D. Thesis, C.I.T., 1954.

10. Mazelsky, Bernard, and O'Connell, Robert F.: Transient Aerodynamic Properties of Wings: Review and Suggested Electrical Representations for Analog Computers. Rep. 11577, Lockheed Aircraft Corp., July 23, 1956.

11. Pines, S., Liban, E., Neuringer, J., and Rabinowitz, S.: The Flutter Analysis of an Elastic Wing with Supersonic Edges. Rep. N. E-SAF-1, Republic Aviation Corp., 1953.

12. Hanson, Perry W., and Tuovila, W. J.: Experimentally Determined Natural Vibration Modes of Some Cantilever-Wing Flutter Models by Using an Acceleration Method. NACA TN 4010, 1957.

13. Garrick, I. E., and Rubinow, S. I.: Theoretical Study of Air Forces on an Oscillating or Steady Thin Wing in a Supersonic Main Stream. NACA Rep. 872, 1947. (Supersedes NACA TN 1383.)

TABLE I.- PHYSICAL CHARACTERISTICS OF DELTA WINGS

Wing	45°	60°
Leading edge sweepback angle, deg	45	60
Trailing edge sweepback angle, deg	0	0
Root chord, in.	6.0	8.5
Semispan, in.	6.0	4.91
Aspect ratio	4.0	2.31
Thickness, in.	0.034	0.034
Material	Magnesium	Magnesium
Weight of semispan, lb	0.0391	0.0453

TABLE II.- EXPERIMENTAL NORMAL MODE AND FLUTTER PROPERTIES OF DELTA WINGS

(a) Normal mode frequencies

Source	45° wing			60° wing		
	f_1	f_2	f_3	f_1	f_2	f_3
Reference 1	49	183	257	67	193	342
	50	185	261	66	200	341
	48	180	273	67	190	338
	48	178	244	66	194	340
	[a]48.8	[a]182	[a]259	[a]66.5	[a]194	[a]340
Reference 12	50	184	258	66	185	336

[a]Average value.

(b) Wind-tunnel flutter characteristics

	45° wing				60° wing			
Mach number	0.40	1.30	2.00	3.00	0.54	1.30	2.00	3.00
v_f, in./sec	0.528	1.54	2.02	2.44×10^4	0.713	1.54	2.02	2.44×10^4
ρ_f, lb sec^2 $in.^{-4}$	1.11	0.318	0.338	0.347×10^{-7}	1.11	0.419	0.338	0.304×10^{-7}
f_f, cps	140	150	159	159	162	172	170	180

TABLE III.- NORMAL MODE FREQUENCIES OF ANALOG STRUCTURE

	Number of cells in analog	45° wing				60° wing			
		Mode 1	Mode 2	Mode 3	Mode 4	Mode 1	Mode 2	Mode 3	Mode 4
Normal mode frequency	21	48.2	182.5	261	430	65.9	190.5	338	395
	15	48.9	183.2	264	430	66.4	192.3	339	389
	10	49.7	188.5	269.5	419	67.5	196.5	345	397
Ratio of analog to model frequency	21	0.987	1.003	1.008	---	0.989	0.982	0.994	---
	15	1.002	1.007	1.019	---	.998	.991	.997	---
	10	1.018	1.036	1.041	---	1.015	1.013	1.014	---

TABLE IV.- NORMAL MODE SHAPES

(a) 45° Cantilever Delta Wing

Cell	10-cell structure				15-cell structure				21-cell structure			
	Mode number											
	1	2	3	4	1	2	3	4	1	2	3	4
	Mode frequency											
	49.7	188.5	269.5	419	48.9	183.2	264	430	48.2	182	261	430
	Vertical deflection, in.											
1	1.000	-0.940	-0.550	0.281	1.000	-0.840	-0.621	-0.422	1.000	-0.978	-0.825	-0.600
2	.600	.004	.858	-.221	.699	-.251	.461	.119	.755	-.459	.255	-.036
3	.482	1.250	-.339	-.940	.598	.585	-.288	1.000	.675	.330	-.396	1.000
4	.241	.265	1.000	.442	.402	.098	1.000	-.140	.518	-.066	1.000	-.016
5	.185	.820	.118	.378	.338	.642	.228	.181	.450	.525	.261	.540
6	.129	1.000	-.468	1.000	.268	1.000	-.429	-.212	.380	1.000	-.429	.492
7					.155	.120	.712	-.360	.291	.110	1.160	-.311
8					.123	.361	.252	-.330	.250	.479	.500	-.128
9					.096	.502	-.129	-.580	.209	.755	-.098	-.321
10					.068	.484	-.319	-.770	.165	.875	-.515	-.780
11									.111	.082	.665	-.320
12									.092	.242	.330	-.295
13									.074	.355	.015	-.426
14									.058	.385	-.200	-.625
15									.041	.331	-.269	-.655
	Angle of twist, θ, radian											
1	(a)	-1.358	0.589	1.110	0.111	-0.990	0.460	-1.357	0.103	-0.996	0.504	-1.614
2		-.915	.892	.531	.092	-.784	.677	-.802	.091	-.845	.693	-1.105
3		-.706	.728	-.068	.092	-.698	.623	-.340	.093	-.801	.655	-.757
4		-.420	.660	.056	.062	-.509	.706	-.286	.071	-.634	.801	-.586
5		-.281	.544	-.204	.062	-.422	.646	.027	.073	-.584	.764	-.271
6		.023	.232	-.189	.063	-.210	.447	.432	.074	-.423	.629	.352
7					.028	-.221	.417	-.027	.046	-.401	.693	-.196
8					.027	-.175	.384	.100	.046	-.357	.666	.005
9					.027	-.058	.258	.200	.047	-.219	.542	.345
10					.026	.074	.066	.008	.047	-.041	.312	.401
11									.021	-.175	.368	-.022
12									.020	-.151	.352	.057
13									.017	-.080	.282	.179
14									.019	.006	.152	.121
15									.019	.088	.008	-.084

[a]Not recorded.

TABLE IV.- NORMAL MODE SHAPES - Concluded.

(b) 60° Cantilever Delta Wing

Cell	10-cell structure				15-cell structure				21-cell structure			
	Mode number											
	1	2	3	4	1	2	3	4	1	2	3	4
	Mode frequency											
	67.5	196.5	345	397	66.4	192.3	339	389	65.9	190.5	338	395
	Vertical bending, in.											
1	1.000	-0.390	-0.722	-0.033	1.000	-0.598	-0.870	0.057	1.000	-0.610	-1.010	0.020
2	.600	-.189	.813	.148	.700	-.378	.375	-.300	.760	-.441	.068	.239
3	.401	1.000	-.028	-.411	.523	.920	.074	1.000	.610	.582	-.020	-.875
4	.241	-.064	1.000	.178	.410	-.200	1.000	-.507	.520	-.290	.840	.420
5	.154	.510	.209	-.088	.299	.679	.402	.440	.410	.508	.425	-.496
6	.078	.481	-.308	1.000	.190	1.000	-.395	-.945	.299	1.000	-.209	.115
7					.159	-.078	.720	-.351	.297	-.166	1.000	.432
8					.111	.318	.311	.100	.229	.350	.548	-.180
9					.070	.443	-.169	-.602	.161	.655	-.060	.280
10					.035	.300	-.250	-.721	.100	.625	-.435	1.000
11									.111	-.069	.581	.250
12									.084	.156	.325	-.031
13									.058	.279	.002	.190
14									.035	.259	-.197	.522
15									.019	.151	-.161	.402
	Angle of twist, θ, radians											
1	0.164	-0.892	-0.028	0.343	0.148	-1.052	-0.199	-0.929	0.138	-0.923	-0.270	0.938
2	.107	-.620	.436	.283	.115	-.849	.203	-.818	.116	-.792	.073	.836
3	.105	-.325	.373	-.328	.116	-.606	.320	.148	.117	-.658	.185	.195
4	.047	-.302	.413	.136	.073	-.563	.391	-.590	.086	-.607	.313	.676
5	.044	-.147	.343	-.213	.071	-.393	.443	.130	.086	-.494	.394	-.130
6	.035	.086	.094	-.137	.065	-.020	.301	.577	.085	-.198	.409	-.643
7					.031	-.253	.264	-.283	.052	-.393	.349	.452
8					.029	-.172	.283	.079	.051	-.312	.400	.065
9					.026	.001	.180	.264	.049	-.109	.367	-.440
10					.019	.111	-.022	-.105	.042	.098	.121	-.233
11									.022	-.174	.202	.211
12									.021	-.134	.223	.021
13									.020	-.041	.196	-.211
14									.018	.042	.073	-.124
15									.013	.073	-.039	.102

TABLE V.- MODULUS OF ELASTICITY INFERRED FROM ANALOG INFLUENCE COEFFICIENTS

Number of cells in analog	Loading point	Deflection point	Inferred modulus of elasticity, lb/sq in.
21	A	A	5.06×10^6
	C	C	5.06
	C	A	4.69
	A	C	4.84
		average	4.91
15	A	A	5.06×10^6
	C	C	5.10
10	A	A	5.13×10^6
	C	C	5.03

TABLE VI.- COMPUTED FLUTTER CHARACTERISTICS

USING STRIP THEORY

		C_{M_q} basic				$C_{M_q} = 0$			
		45° wing		60° wing		45° wing		60° wing	
Mach number		2.0	3.0	2.0	3.0	2.0	3.0	2.0	3.0
Flutter frequency, cps	Analog	132	131	132	130	144	142	152	149
	Experimental	159	159	170	180	159	159	170	180
	Ratio	0.83	0.82	0.78	0.72	0.91	0.89	0.89	0.83
Dynamic pressure, $\frac{\rho v^2}{2}$, lb/sq in.	Analog	5.76	9.37	4.19	6.85	----	----	----	----
	Experimental	6.86	10.3	6.86	9.02	----	----	----	----
Flutter parameter, Ψ, lb/sq in.	Analog	13.4	13.3	9.70	9.73	13.2	13.3	9.85	10.0
	Experimental	15.9	14.6	15.9	12.8	15.9	14.6	15.9	12.8
	Ratio	0.84	0.91	0.61	0.76	0.83	0.91	0.62	0.78

TABLE VII.- FLUTTER CHARACTERISTICS USING STRIP THEORY

(a) Effect of Aerodynamic Center

Strip	45° wing		60° wing	
	$\dfrac{\Delta \frac{\rho v^2}{2} \Big/ \frac{\rho v^2}{2}}{\Delta x_o}$ (a)	$\dfrac{\Delta f_f / f_f}{\Delta x_o}$ (a)	$\dfrac{\Delta \frac{\rho v^2}{2} \Big/ \frac{\rho v^2}{2}}{\Delta x_o}$ (a)	$\dfrac{\Delta f_f / f_f}{\Delta x_o}$ (a)
Tip 1	1.2	0.11	1.1	0.15
2	3.5	.61	2.3	.48
3	3.6	.92	1.3	.45
4	.6	.15	.1	.02
Root 5	0	0	0	0

[a]Note that $\Delta \frac{\rho v^2}{2}$ and Δf_f are positive for Δx_o positive (aft).

(b) Effect of Reference Axis x_1

Strip	45° wing	60° wing
	$\dfrac{\Delta \frac{\rho v^2}{2} \Big/ \frac{\rho v^2}{2}}{\Delta x_1}$ (a)	$\dfrac{\Delta \frac{\rho v^2}{2} \Big/ \frac{\rho v^2}{2}}{\Delta x_1}$ (a)
1	0	0
2	.03	.1
3	.03	.1
4	.02	.03
5	0	0

[a]Note that $\Delta \frac{\rho v^2}{2}$ is positive for Δx_1 positive (aft).

TABLE VIII.- COMPUTED FLUTTER CHARACTERISTICS USING BOX METHOD

		45° wing			60° wing	
Mach number		1.5	2.0	3.0	2.0	3.0
Case A						
Flutter frequency, cps	Analog 10 cell . . .	174	171	169	183	181
	15 cell . . .	166	163	162	180	177
	21 cell . . .	161	159	158	177	175
	Experimental	[a]152	159	159	170	180
Dynamic pressure, $\frac{\rho v^2}{2}$ lb/sq in.	Analog 10 cell . . .	6.19	9.22	14.7	8.44	13.5
	15 cell . . .	5.78	8.41	13.6	8.23	13.2
	21 cell . . .	5.39	8.19	13.1	8.10	13.1
	Experimental	[a]4.65	6.86	10.3	6.86	9.02
Flutter parameter, $\bar{\Psi}$ lb/sq in.	Analog 10 cell . . .	22.1	21.3	20.8	19.5	19.1
	15 cell . . .	20.7	19.4	19.2	19.0	18.6
	21 cell . . .	19.3	18.9	18.6	18.7	18.5
	Experimental	[a]16.6	15.9	14.6	15.9	12.8
$\frac{\bar{\Psi}_{analog}}{\bar{\Psi}_{exper.}}$	10 cell . . .	1.33	1.35	1.43	1.23	1.49
	15 cell . . .	1.23	1.24	1.33	1.20	1.46
	21 cell . . .	1.16	1.20	1.27	1.18	1.45
Case B						
Flutter frequency, cps	Analog 10 cell . . .	167	166	167	179	178
	15 cell . . .	162	159	160	177	175
	21 cell . . .	158	158	156	175	173
	Experimental	152	159	159	170	180
Dynamic pressure, $\frac{\rho v^2}{2}$ lb/sq in.	Analog 10 cell . . .	4.84	7.68	13.6	7.61	12.5
	15 cell . . .	4.61	7.34	12.7	7.41	12.3
	21 cell . . .	4.42	7.41	12.4	7.26	12.2
	Experimental	4.65	6.86	10.3	6.86	9.02
Flutter parameter, $\bar{\Psi}$ lb/sq in.	Analog 10 cell . . .	17.3	17.8	19.3	17.6	17.7
	15 cell . . .	16.4	17.0	17.9	17.2	17.4
	21 cell . . .	15.8	17.2	17.5	16.9	17.3
	Experimental	16.6	15.9	14.6	15.9	12.8
$\frac{\bar{\Psi}_{analog}}{\bar{\Psi}_{exper.}}$	10 cell . . .	1.04	1.12	1.32	1.11	1.38
	15 cell . . .	.99	1.07	1.23	1.08	1.36
	21 cell . . .	.95	1.08	1.20	1.06	1.35
Case C						
Flutter frequency, cps	15 cell . . .	157	159	(b)	172	173
$\frac{\bar{\Psi}_{analog}}{\bar{\Psi}_{exper.}}$	15 cell . . .	.965	1.06	(b)	1.05	1.35

[a]Obtained by interpolation.

[b]Tests not made.

TABLE IX.- THREE-DIMENSIONAL PRESSURE INTERACTIONS USING BOX METHOD

[All other nonzero interactions are contained in this table. For example, reference to figure 5 shows that

$$P_{7,6} = P_{2,6}$$

In addition, if symmetric motion is assumed, there are contributions from cells on the other side of wing center line. Thus $P_{7,15}$ should contain both interactions (7,15) and (1,15) listed below, the first due to motion of cell 15 and the second due to motion of its mirror image across center line.]

Interaction (i,j)	45° wing						60° wing			
	P_0			$\frac{P_1}{\beta^2\Delta x}$			P_0		$\frac{P_1}{\beta^2\Delta x}$	
	Mach number			Mach number			Mach number		Mach number	
	1.5	2.0	3.0	1.5	2.0	3.0	2.0	3.0	2.0	3.0
(1, 1)	1.000	1.000	1.000	-0.267	-0.0833	-0.021	1.000	1.000	-0.083	-0.021
(1, 3)	.378	.304	.108	-.498	-.234	-.059	.392	.317	-.238	-.125
(1, 6)	.266	0	-----	-.694	0	0	.295	.064	-.385	-.060
(1, 10)	.206	0	0	-.797	0	0	.247	0	-.489	0
(1, 15)	.164	0	0	-.844	0	0	.216	0	-.574	0
(2, 3)	-.757	-.608	-.216	.463	.301	.076	-.784	-.634	.310	.209
(2, 6)	-.216	.083	.200	.363	-.165	-.149	-.251	.013	.260	-.011
(2, 10)	-.131	.234	0	.369	-.472	0	-.183	.189	.309	-.210
(2, 15)	-.083	.088	0	.327	-.259	0	-.151	.138	.354	-.220
(4, 6)	-.100	-.167	-.401	.130	.164	.256	-.088	-.155	.085	.100
(4, 10)	-.054	-.201	.059	.121	.340	-.079	-.045	-.158	.070	.159
(4, 15)	-.044	-.017	.108	.145	.029	-.177	-.033	-.075	.070	.114
(7, 10)	-.041	-.066	-.118	.082	.098	.117	-.037	-.062	.054	.061
(7, 15)	-.026	-.052	-.078	.075	.111	.115	-.023	-.047	.046	.063
(11, 15)	-.023	-.036	-.061	.061	.071	.082	-.020	-.034	.040	.045

TABLE X.- EFFECT OF INDIVIDUAL AERODYNAMIC INTERACTIONS

ON FLUTTER PARAMETER, $\frac{\rho V^2}{2}$

[Interaction (i-j) denotes force acting on cell (j) due to motion of cell (i). Quantities k_1 and k_2 are defined in text.]

45° wing; Mach 2.0; 15 cell case		
Interaction	k_1	k_2
1-1	0.27	0.16
3-1	.07	.17
2-2	0.44	0.30
3-2	-.25	.30
5-2	.06	.25
6-2	.02	.27
10-2	.01	.16
3-3	-0.72	-0.53
6-3	-.09	-.42
3-4	0.12	0.29
4-4	.29	.31
5-4	-.17	.32
6-4	-.04	.29
8-4	.03	.29
9-4	.01	.23
10-4	-.01	.27
5-5	-0.27	-0.31
6-5	.13	-.30
9-5	-.02	-.22
10-5	-.002	-.17
6-6	-0.73	-1.0
10-6	-.04	-.93
5-7	0.05	0.20
6-7	.01	.19
7-7	.08	.20
8-7	-.05	.20
9-7	-.01	.15
10-7	-.001	.07
6-8	-0.01	-0.06
8-8	-.02	-.06
9-8	.01	-.05
10-8	.001	-.05
9-9	-0.12	-0.41
10-9	.03	-.37
10-10	-0.09	-0.69

TABLE XI.- EFFECT OF CENTER OF PRESSURE OF EACH CELL ON FLUTTER PARAMETER, $\rho v^2/2$

[The term Δx is cell length in airstream direction and $\frac{\Delta c.p.}{\Delta x}$ is the shift forward of center of pressure expressed as per unit value of Δx.]

45° wing; 15 cell; Mach 3.0; case A	
Cell	$\frac{\frac{\Delta \rho v^2/2}{\rho v^2/2}}{\frac{\Delta c.p.}{\Delta x}}$
1	-1.60
2	-1.44
3	-1.78
4	-.63
5	-.82
6	-.55
7	-.13
8	-.16
9	-.09
10	.00
11	.00
12	.00
13	.00
14	.00
15	.00

TABLE XII.- APPROXIMATE FLUTTER MODE SHAPES

Cell	45° wing		60° wing	
	Vertical deflection			
	Amplitude, in.	Phase, deg	Amplitude, in.	Phase, deg (a)
1	1.00	0	1.00	-
2	.65	1	.67	-
3	.43	3	.32	-
4	.36	2	.38	-
5	.21	7	.17	-
6	.11	17	.06	-
7	.12	5	.15	-
8	.07	15	.06	-
9	.03	36	.02	-
10	.02	80	.01	-
11	0	0	0	-
12	0	0	0	-
13	0	0	0	-
14	0	0	0	-
15	0	0	0	-
Cell	Angle of twist			
	Amplitude, radians	Phase, deg (a)	Amplitude, radians (a)	Phase, deg (a)
1	0.25	-	-	-
2	.21	-	-	-
3	.18	-	-	-
4	.13	-	-	-
5	.12	-	-	-
6	.07	-	-	-
7	.06	-	-	-
8	.04	-	-	-
9	.02	-	-	-
10	.01	-	-	-
11	0	-	-	-
12	0	-	-	-
13	0	-	-	-
14	0	-	-	-
15	0	-	-	-

[a]Not measured.

TABLE XIII.- DIGITAL FLUTTER COMPUTATIONS

	45° wing				60° wing			
	Mach 2.0		Mach 3.0		Mach 2.0		Mach 3.0	
	Ψ, lb/sq in.	f_f, cps	Ψ, lb/ sq in.	f_f, cps	Ψ, lb/sq in.	f_f, cps	Ψ, lb/sq in.	f_f, cps
[a]Experimental	15.8	159	14.6	159	15.8	170	12.8	180
Analog, 15 cell	19.4	163	19.2	162	19.0	180	18.6	177
Two modes	15.04	150.7	14.91	150.5	15.90	171.3	15.72	171.0
Three modes	-----	-----	17.86	160	-----	-----	17.65	178
Four modes	-----	-----	18.74	164.7	-----	-----	-----	-----

[a]Based on experimental values of v and ρ and theoretical average lift coefficient $4/\beta$.

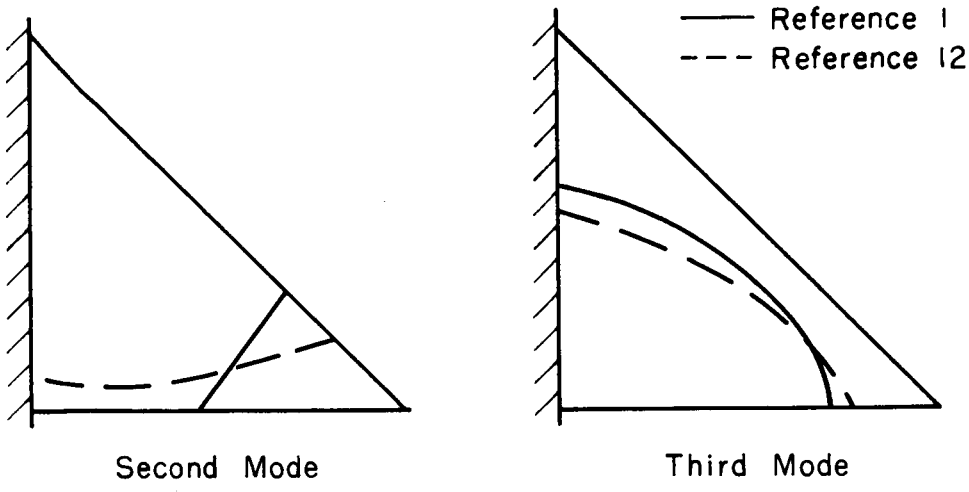

(a) 45° wing.

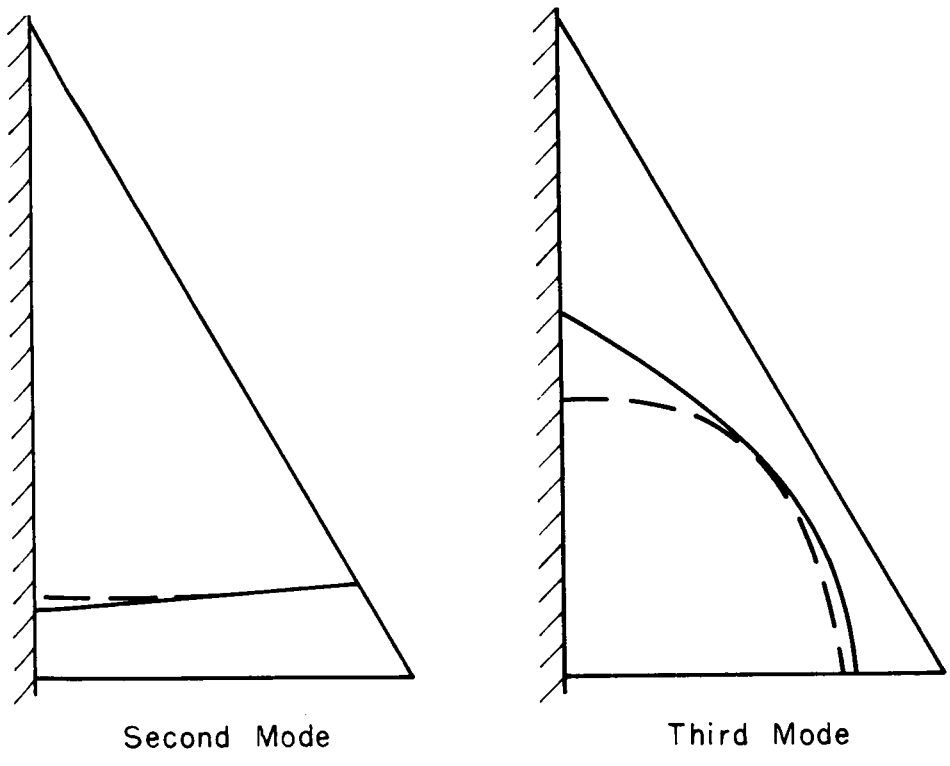

(b) 60° wing.

Figure 1.- Plan forms and experimental normal mode node lines for delta wings.

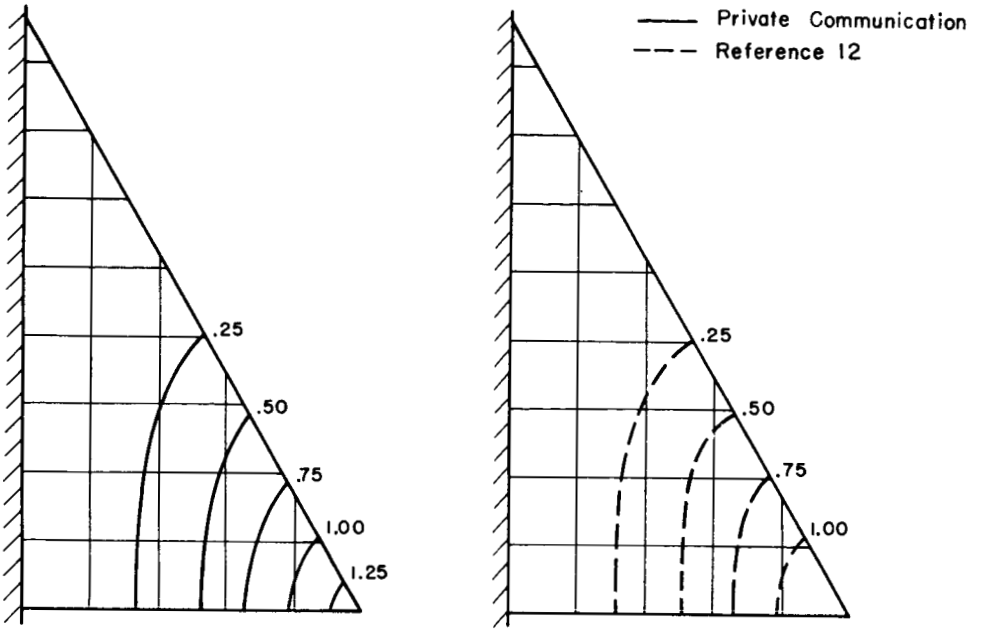

(a) First mode; f_1 = 66 cps.

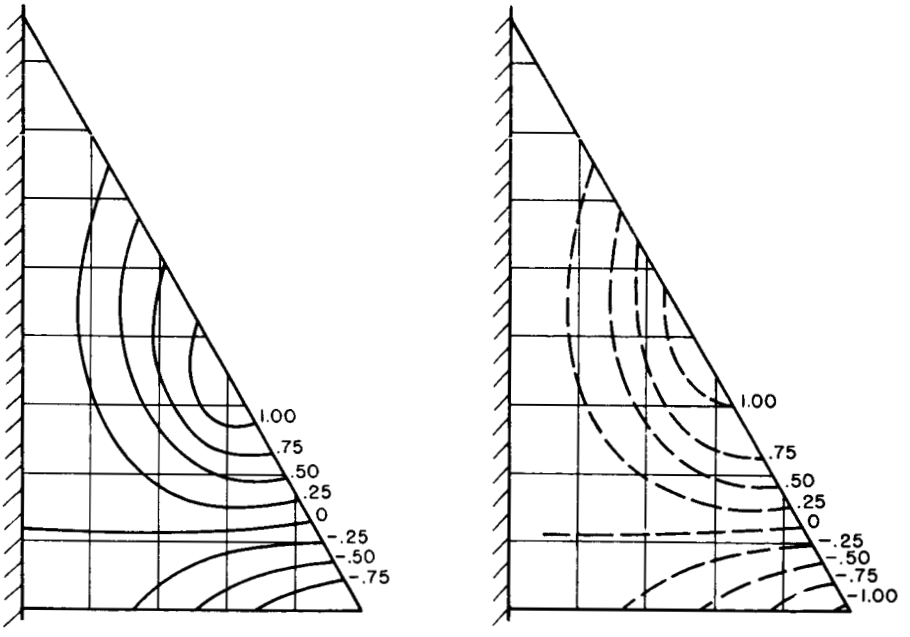

(b) Second mode; f_2 = 185 cps.

Figure 2.- Experimental mode shapes of 60° wing.

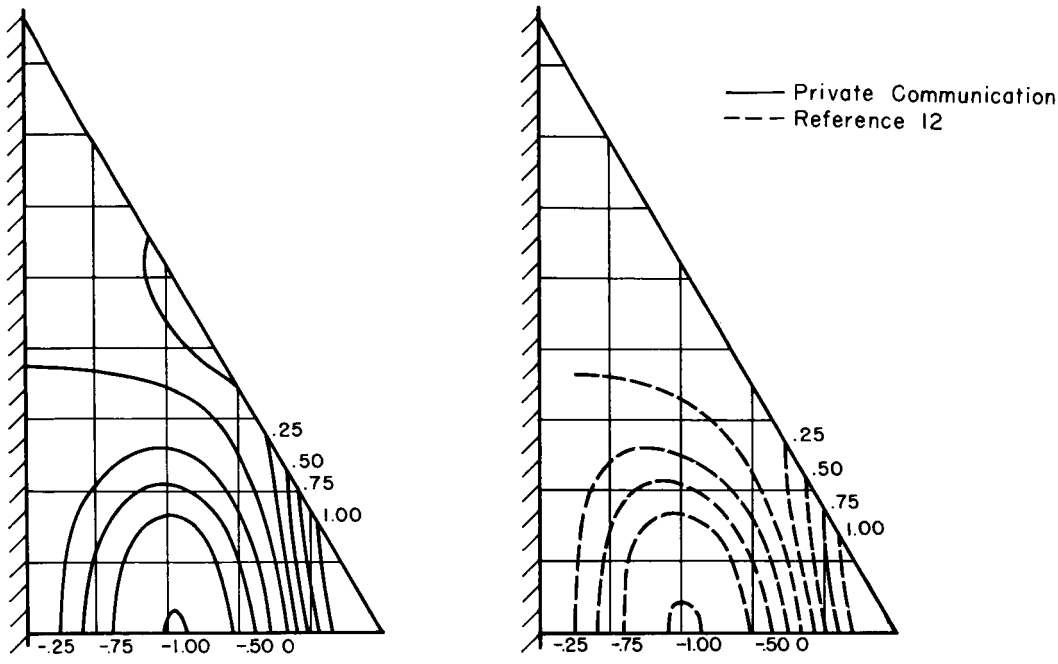

(c) Third mode; f_3 = 336 cps.

Figure 2.- Concluded.

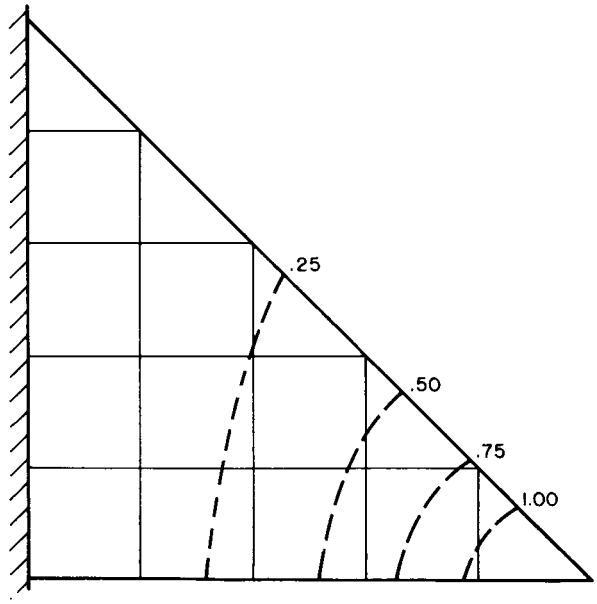

(a) First mode; f_1 = 50 cps.

Figure 3.- Experimental mode shapes for 45° wing (ref. 12).

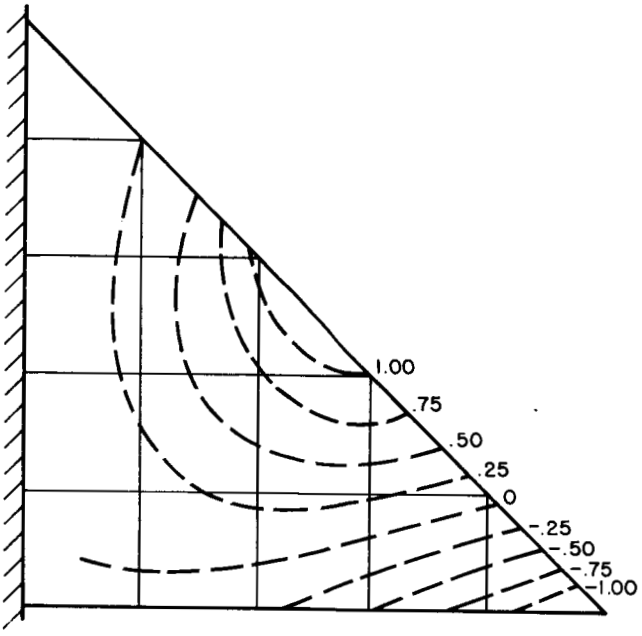

(b) Second mode; f_2 = 184 cps.

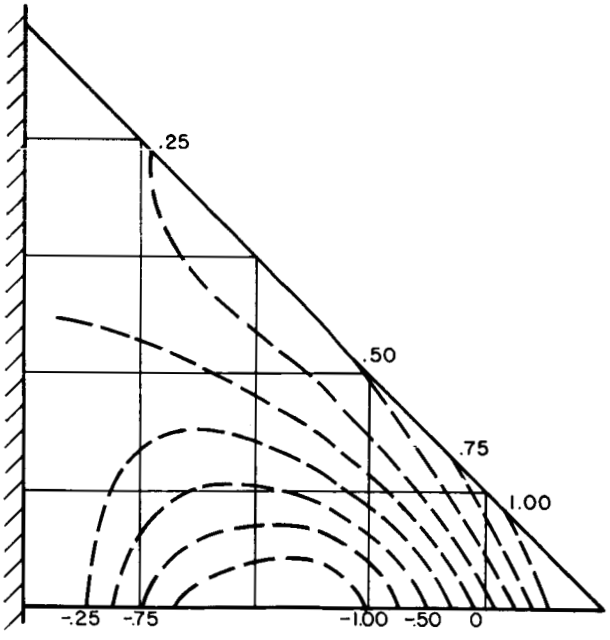

(c) Third mode; f_3 = 258 cps.

Figure 3.- Concluded.

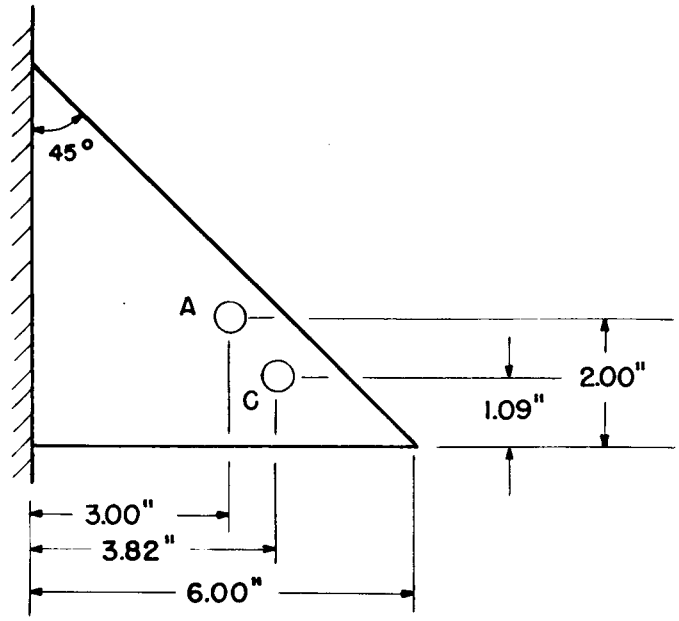

		Influence coefficient at loading point, in./lb	
		A	C
Deflection point	A	0.123	0.181
	C	.175	.292

Figure 4.- Experimental influence coefficients of 45° wing.

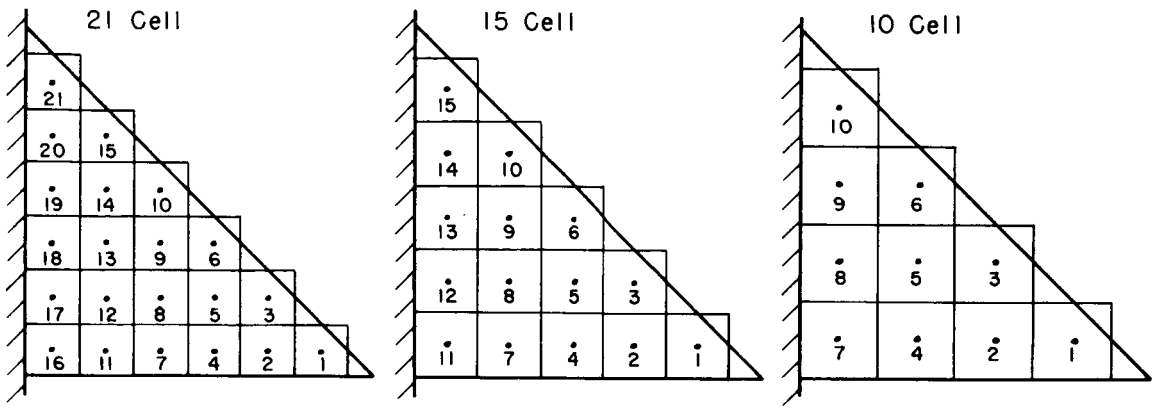

(a) 45° delta wing.

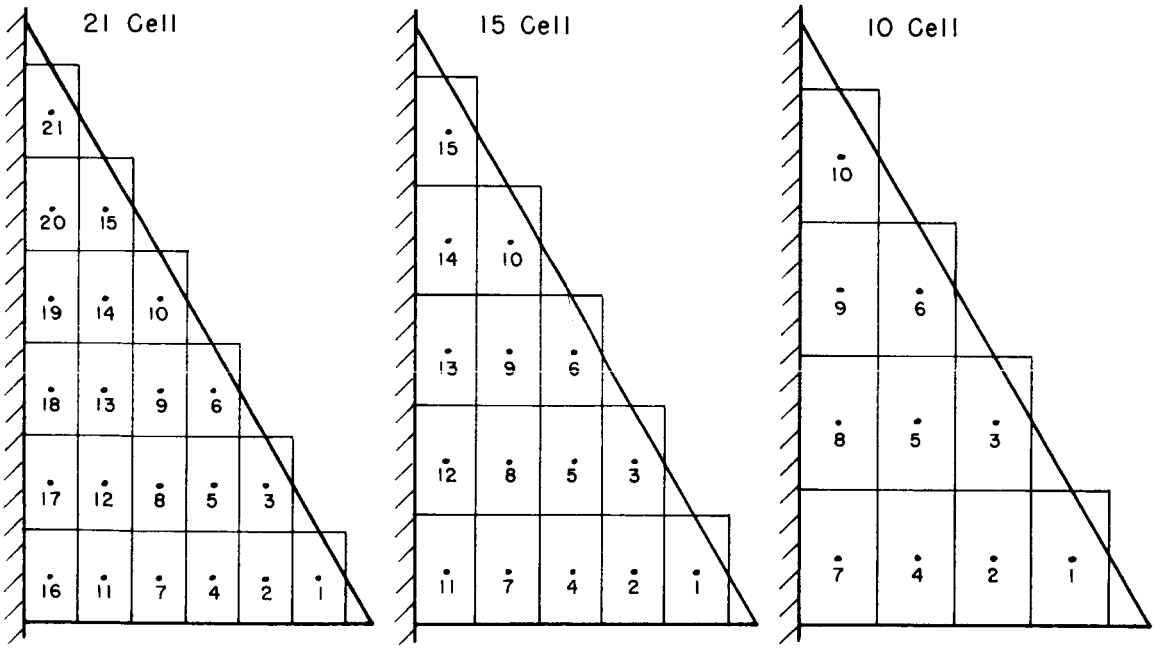

(b) 60° delta wing.

Figure 5.- Cell divisions used for analog representation. Dots are points at which deflection is defined in analog circuit.

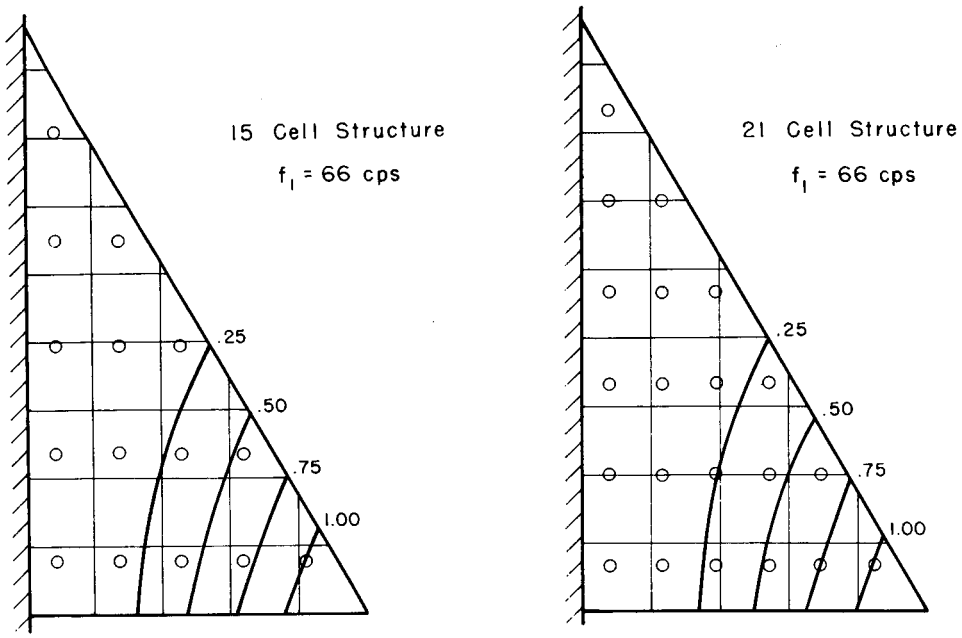

(a) First mode.

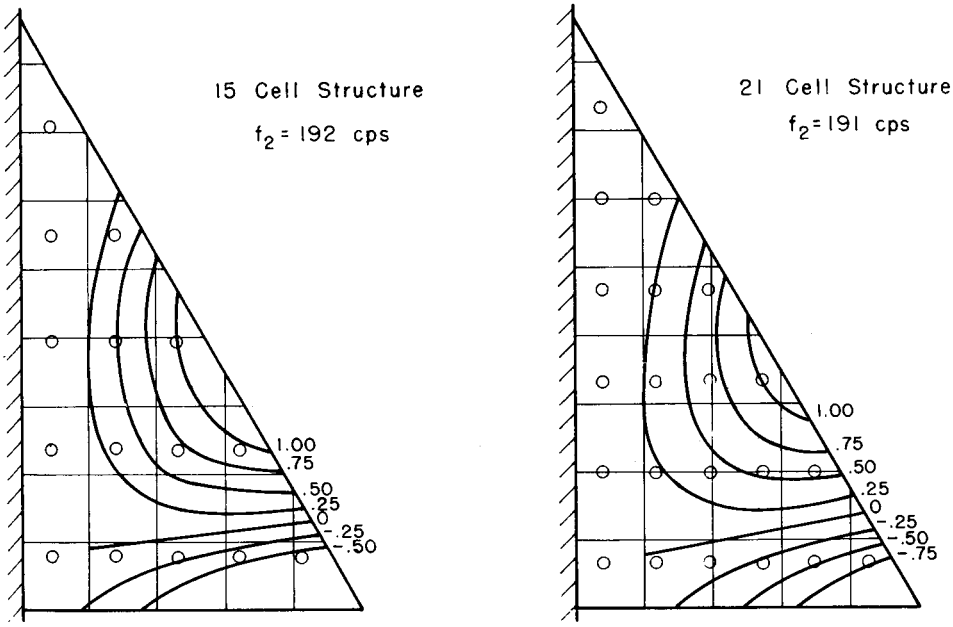

(b) Second mode.

Figure 6.- Analog mode shapes for 60° wing.

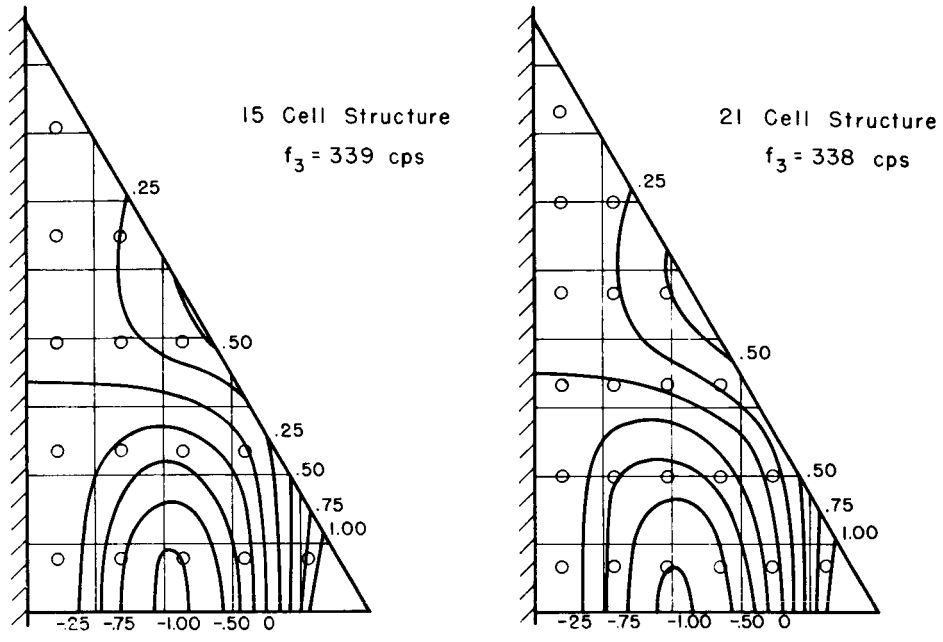

(c) Third mode.

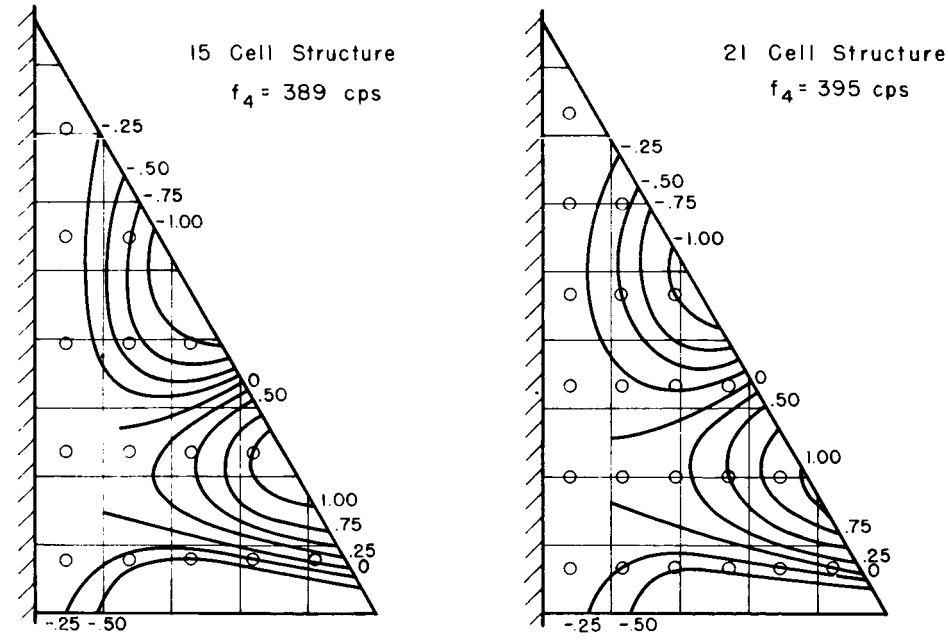

(d) Fourth mode.

Figure 6.- Concluded.

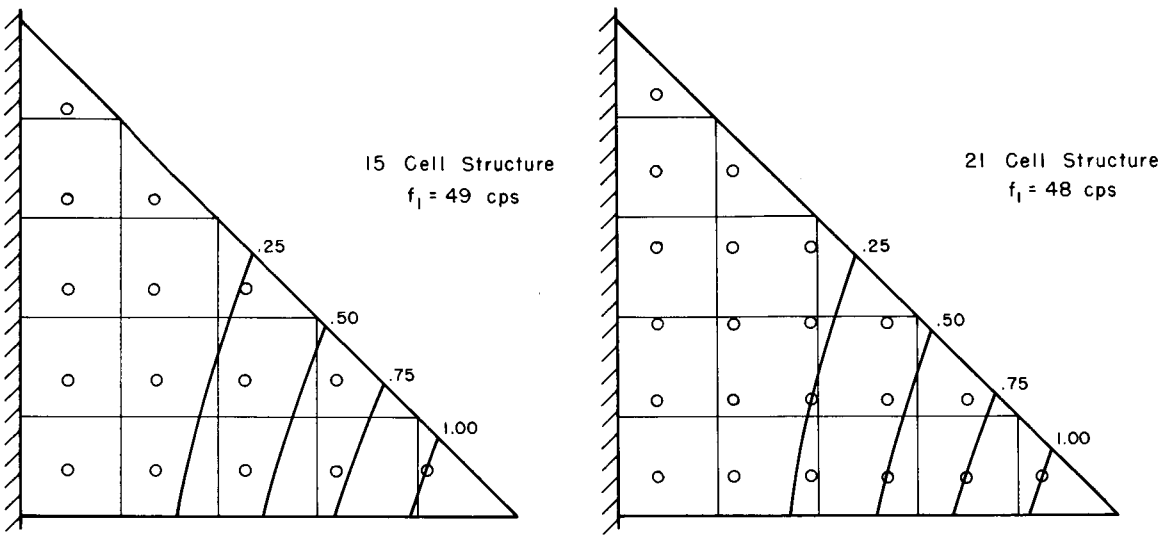

(a) First mode.

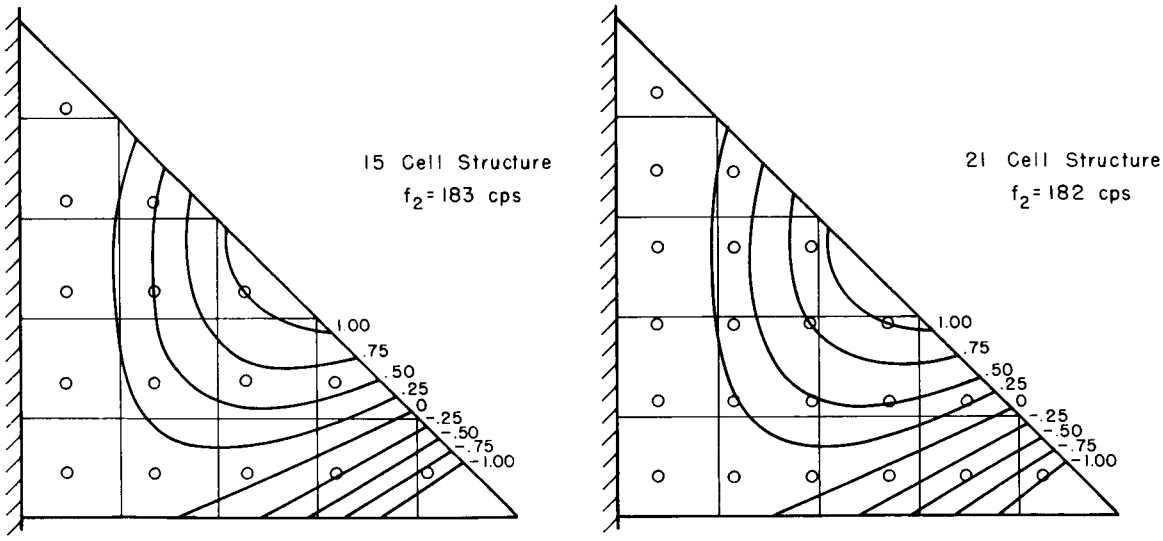

(b) Second mode.

Figure 7.- Analog mode shapes for 45° wing.

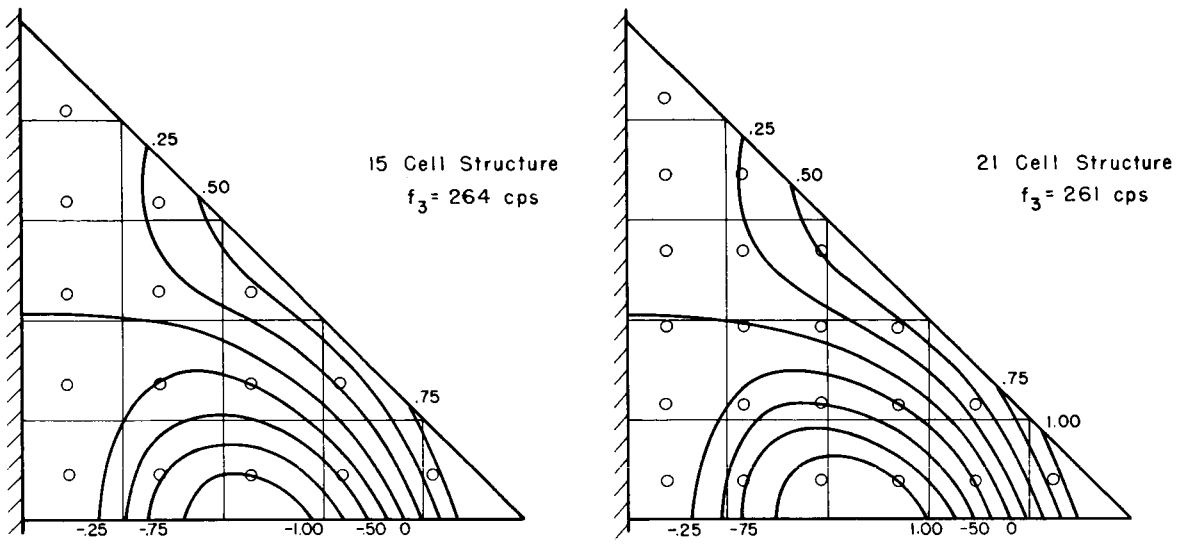

(c) Third mode.

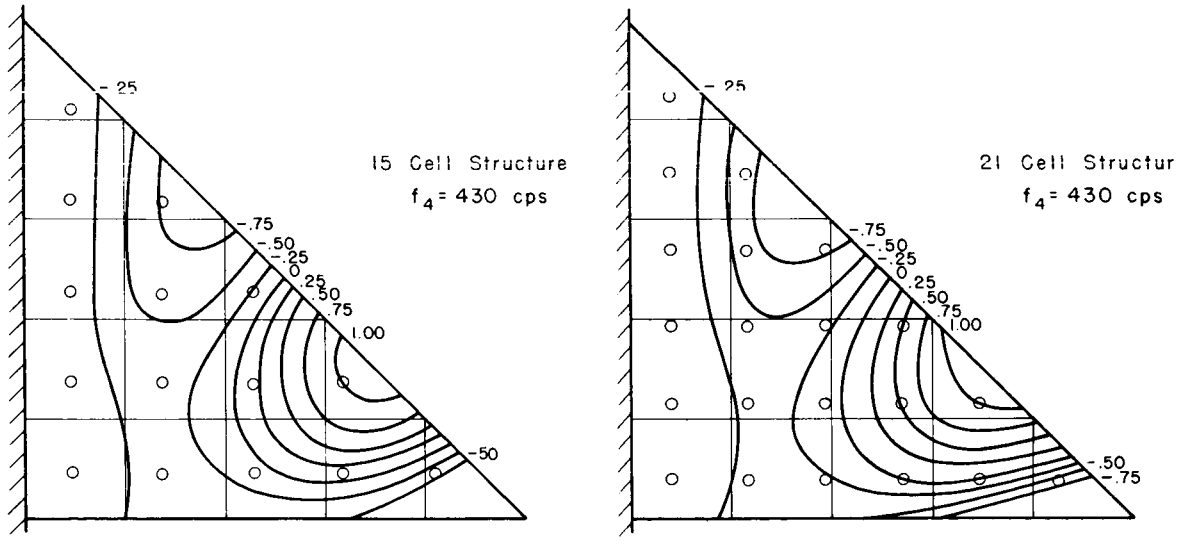

(d) Fourth mode.

Figure 7.- Concluded.

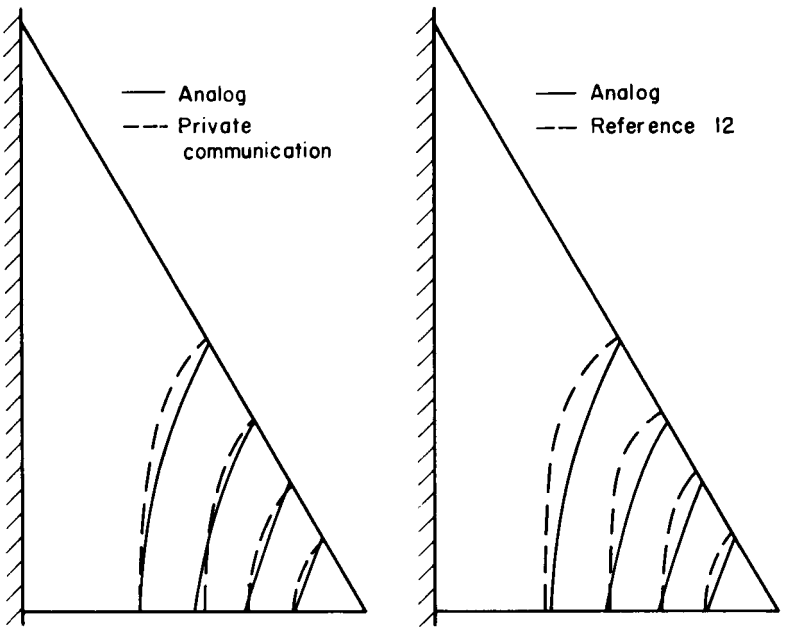

(a) First mode.

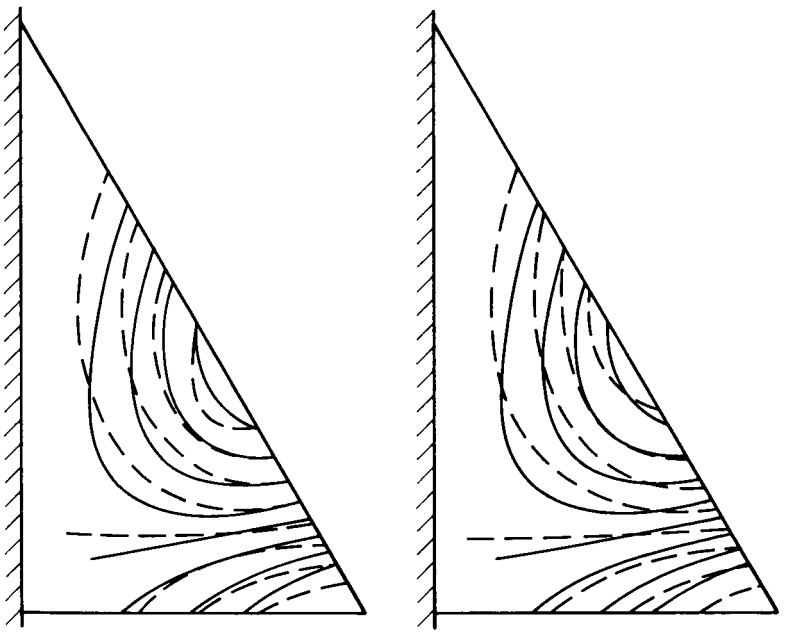

(b) Second mode.

Figure 8.- Comparison of experimental and analog mode shapes for 60° wing.

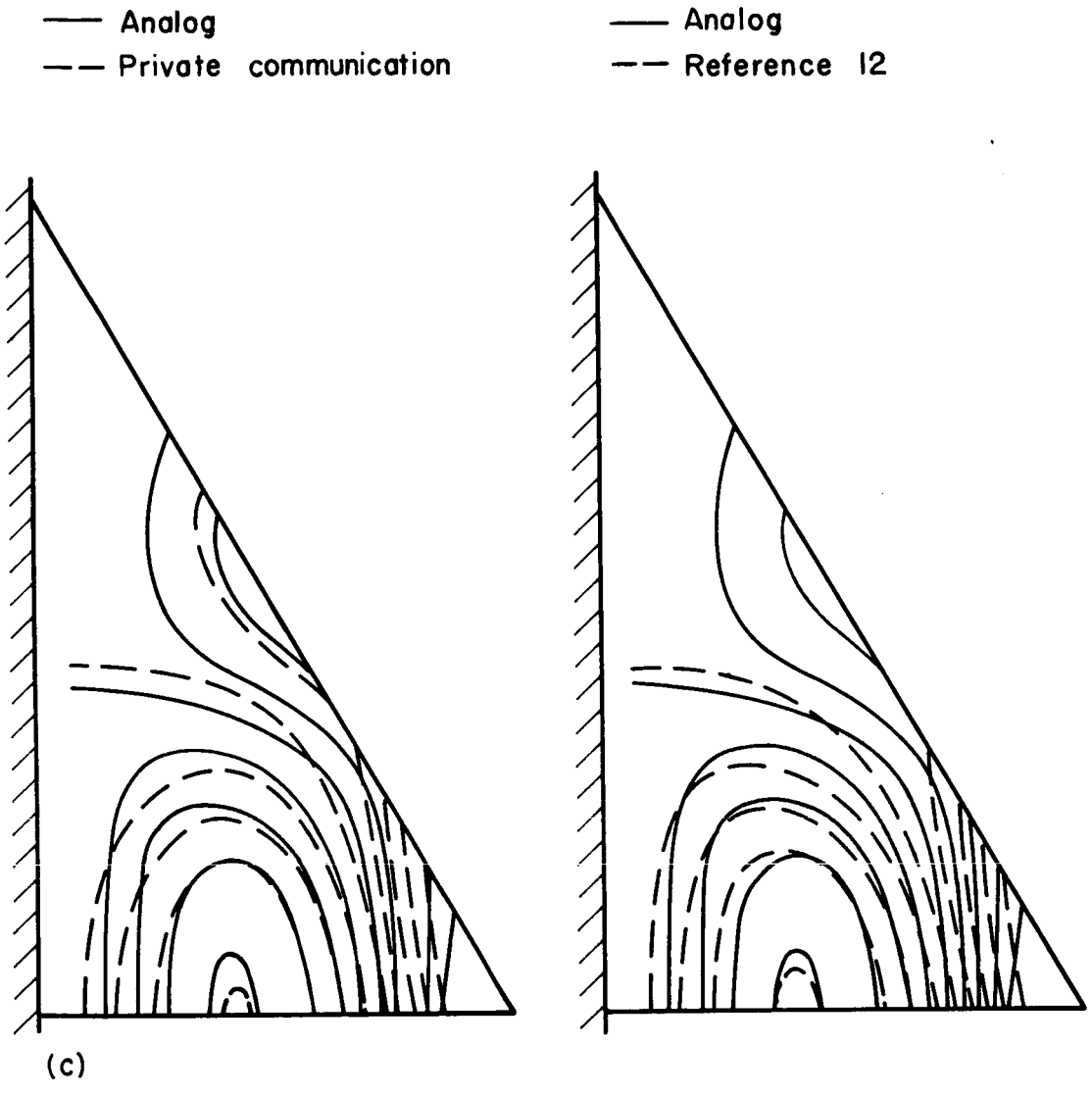

(c) Third mode.

Figure 8.- Concluded.

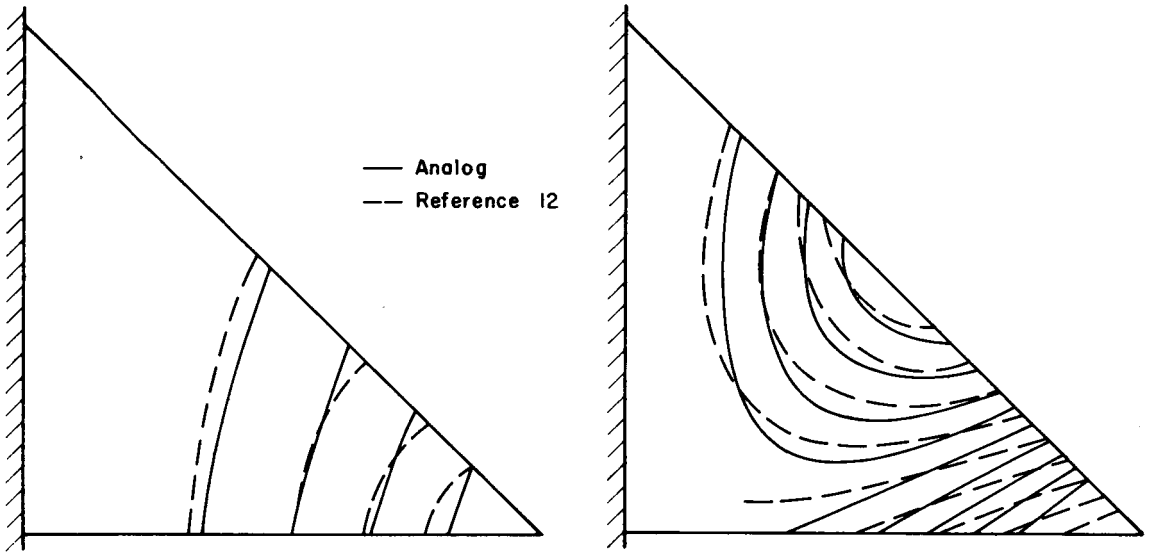

(a) First mode.

(b) Second mode.

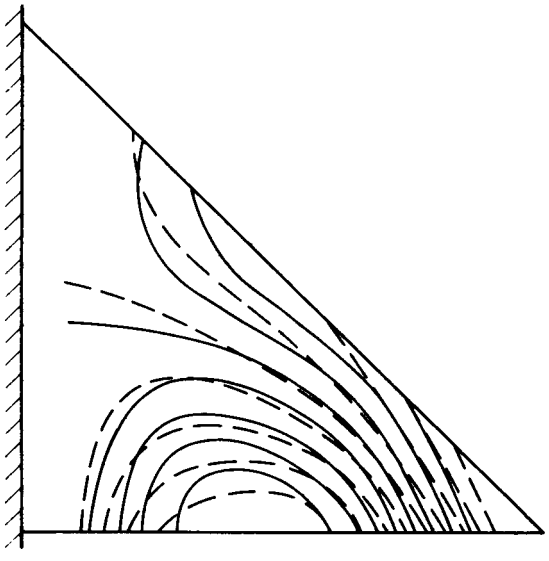

(c) Third mode.

Figure 9.- Comparison of experimental and analog mode shapes for 45° wing.

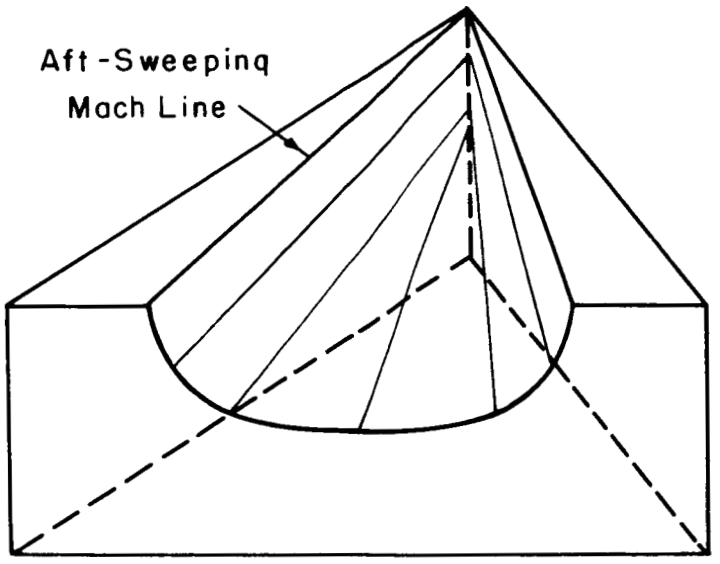

(a) Three-dimensional sketch of pressure distribution.

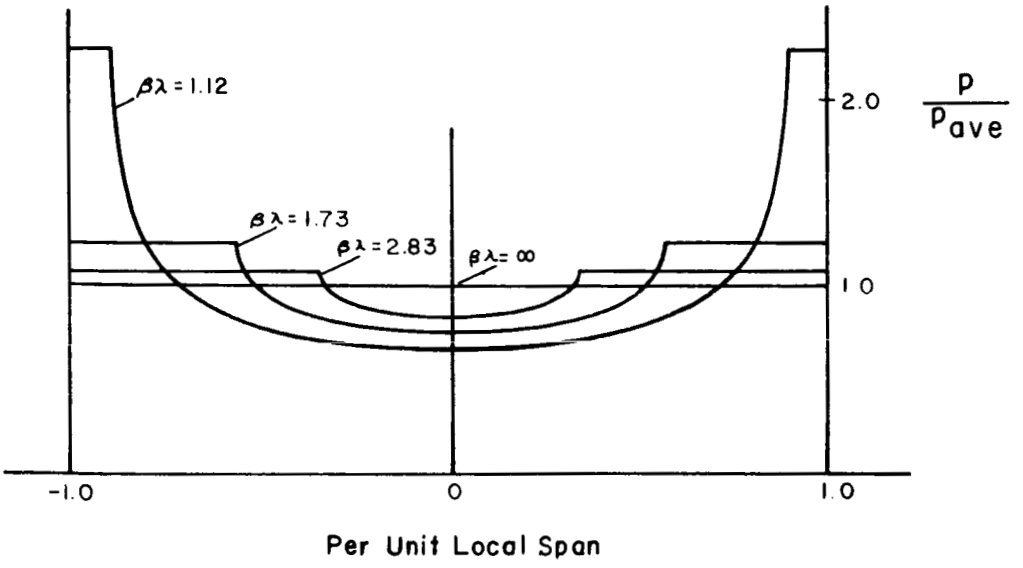

(b) Typical cross section.

Figure 10.- Static pressure distribution on rigid delta wing with supersonic leading edge. $p_{ave} = \left(\frac{\rho v^2}{2}\right)\left(\frac{4}{\beta}\right)(\alpha)$; $p_{max} = \frac{\beta\lambda}{\sqrt{\beta^2\lambda^2 - 1}}\left(p_{ave}\right)$; $p_{min} = \frac{2}{\pi}\tan^{-1}\sqrt{\beta^2\lambda^2 - 1}\,\left(p_{max}\right)$.

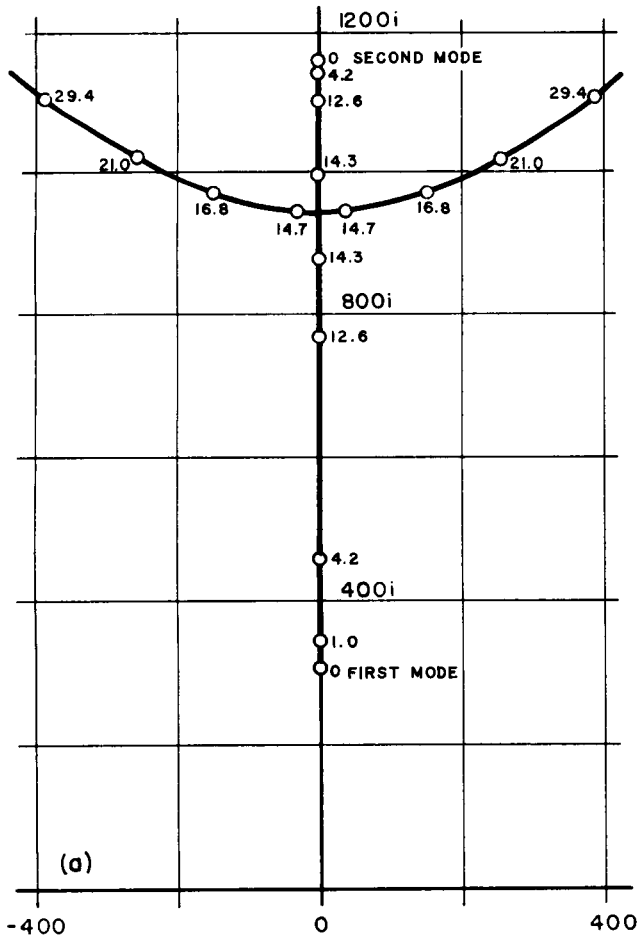

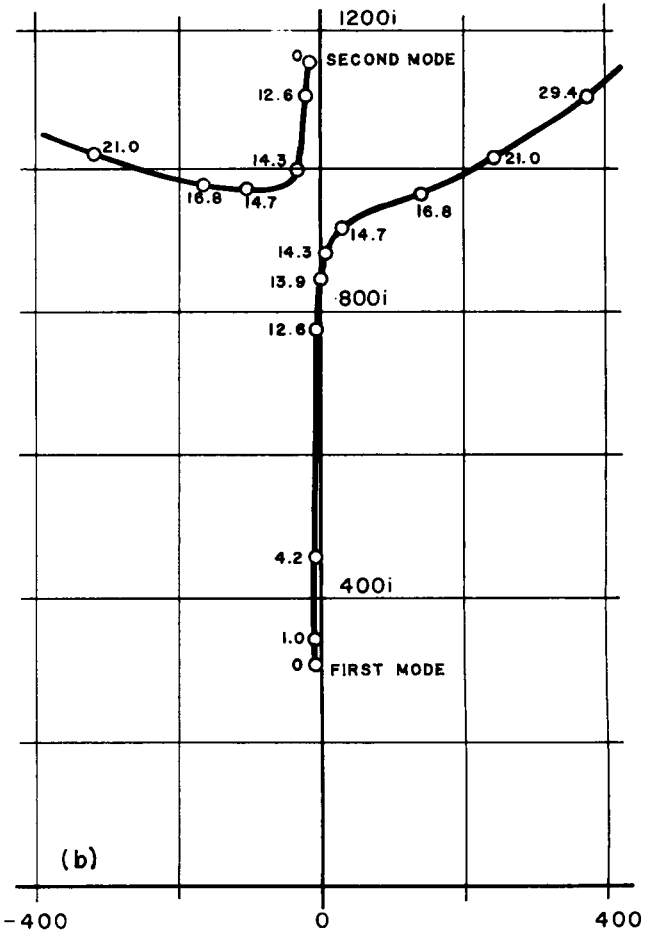

(a) $P_j = \Psi\, \Delta S_j(\theta_j)$; $g_1 = 0$, $g_2 = 0$.

(b) $P_j = \Psi\, \Delta S_j(\theta_j)$; $g_1 = 0.05$, $g_2 = 0.03$.

Figure 11.- Location of flutter roots in complex plane as functions of Ψ. Small numbers indicate value of Ψ.

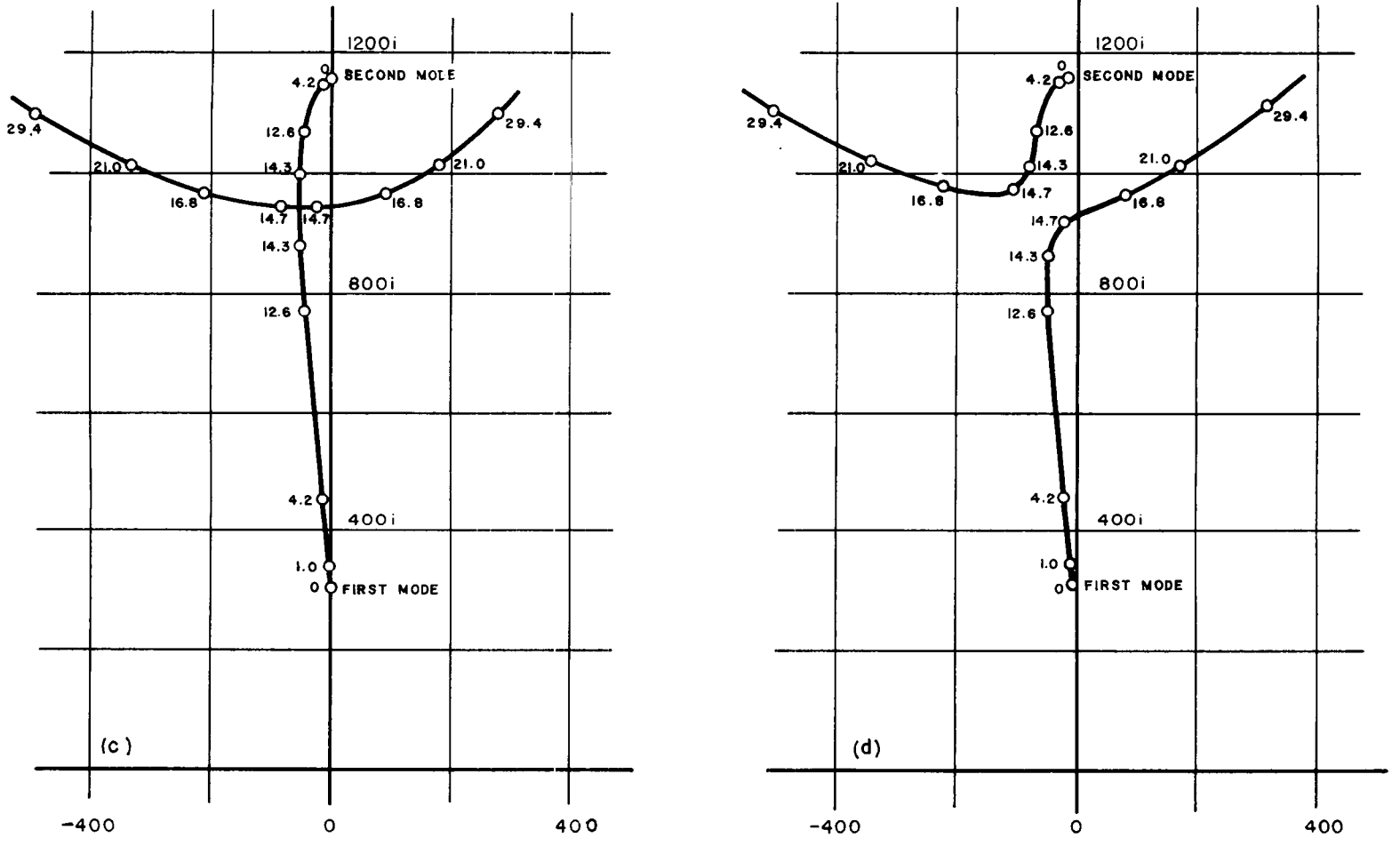

(c) $P_j = \Psi \Delta S_j \left(\theta + \frac{\dot{h}}{V}\right)_j$; $g_1 = 0$, $g_2 = 0$.

(d) $P_j = \Psi \Delta S_j \left(\theta + \frac{\dot{h}}{V}\right)_j$; $g_1 = 0.05$, $g_2 = 0.03$.

Figure 11.- Concluded.

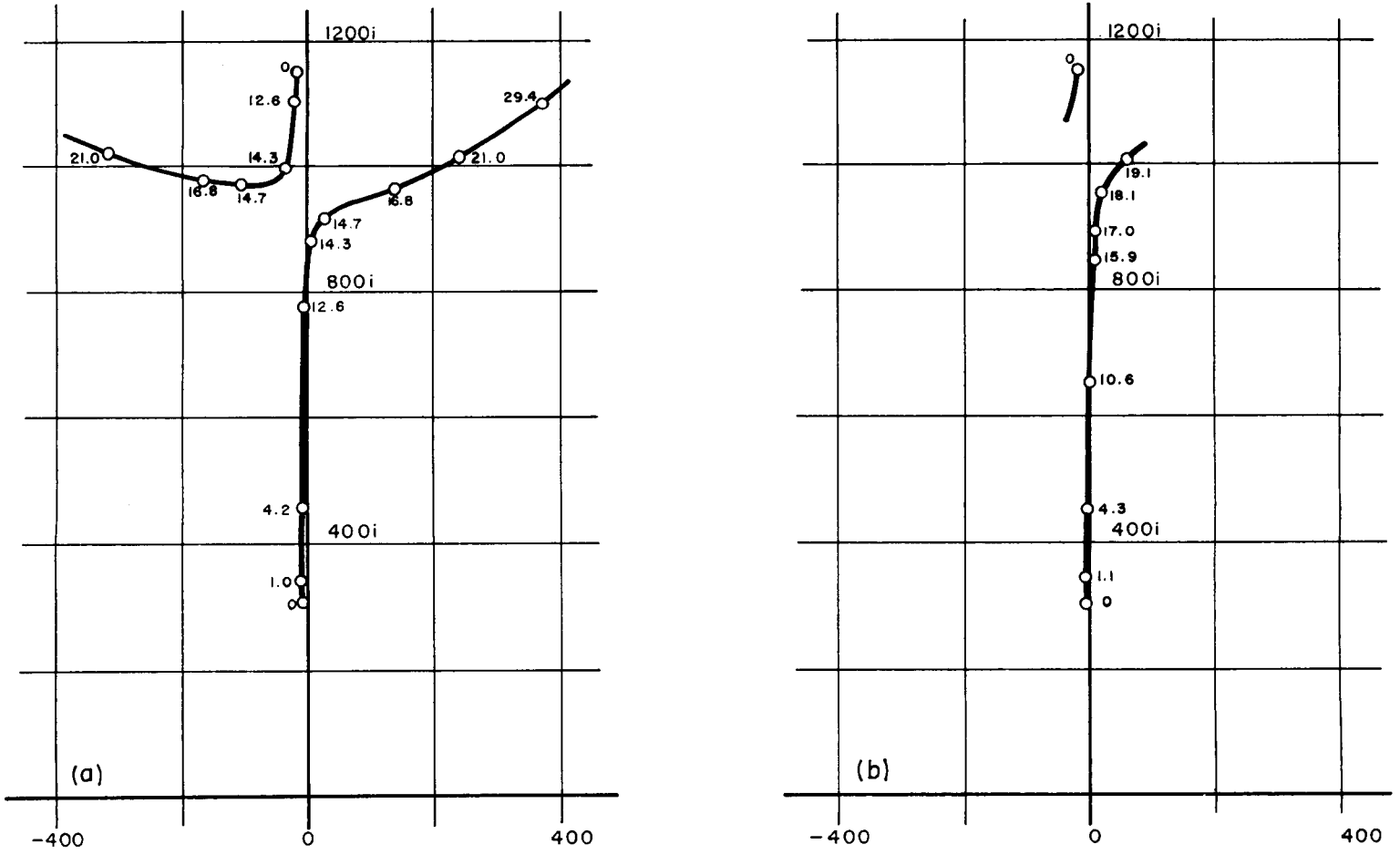

(a) Digital computer, 2 modes.

(b) Analog computer, 15 cells.

Figure 12.- Comparison of analog and digital computations. Small numbers indicate value of Ψ. $P_j = \Psi\, \Delta S_j\left(\theta_j\right)$; $g_1 = 0.05$; $g_2 = 0.03$.

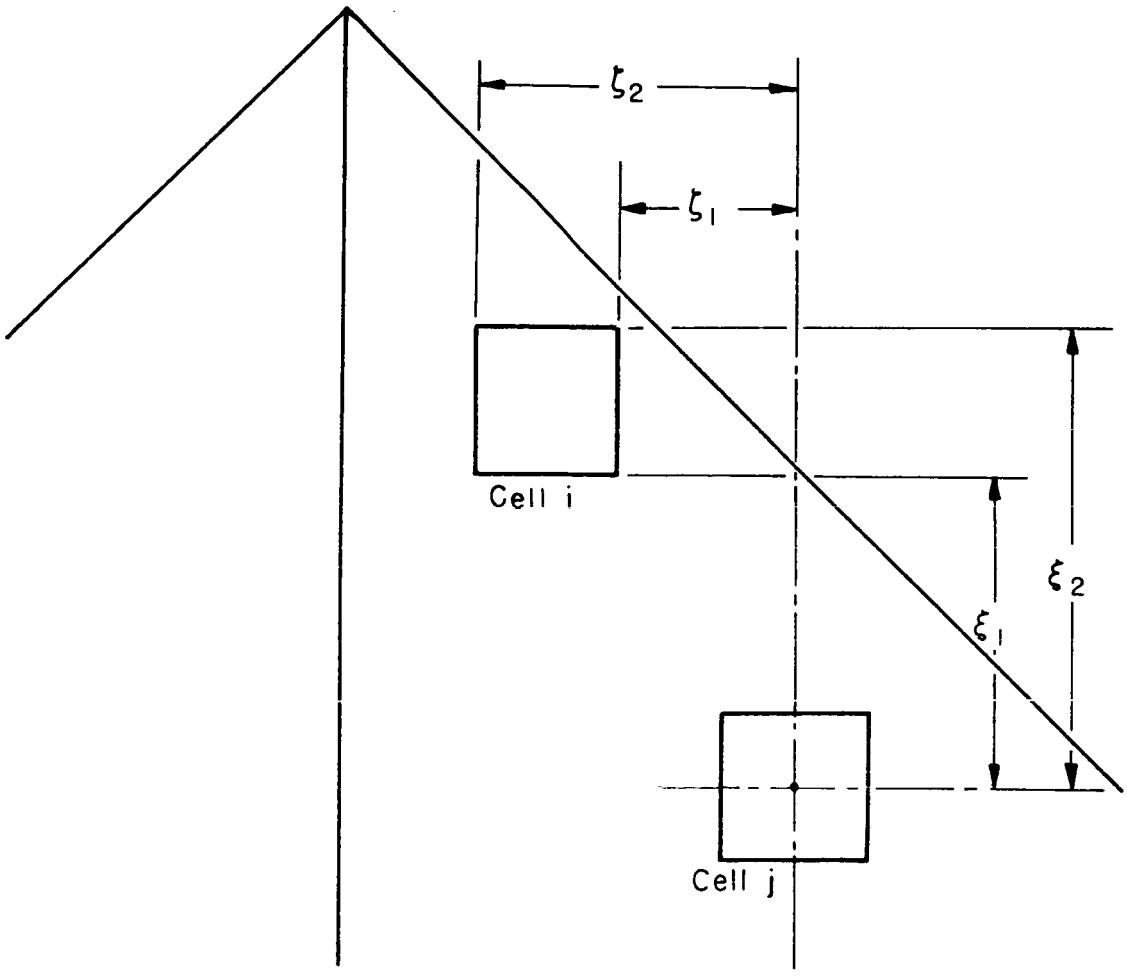

Figure 13.- Wing-relative coordinates for defining three-dimensional pressure interactions.